Materials Advances

ROYAL SOCIETY OF CHEMISTRY

REVIEW

View Article Online
View Journal | View Issue

Cite this: *Mater. Adv.*, 2022, 3, 8864

Signal amplification strategies in electrochemical biosensors *via* antibody immobilization and nanomaterial-based transducers

Mitkumar Patel,† Mayuri Agrawal† and Akshay Srivastava *

The electrochemical biosensor has higher sensitivity and selectivity and has the potential to facilitate rapid detection for the diagnosis of diseases. Sample preparation, detection time, and real-time sensing are some of the major limitations associated with the detection of disease, especially in the early stages. Because of their enhanced selectivity, superior signal-to-noise ratios, and the necessity of extremely tiny sample quantities, electrochemical biosensors have become a stepping stone for early disease diagnosis in recent years. The combination of materials science and electrochemistry has decisively contributed to the field of developing highly sensitive electrochemical sensors. A tremendous amount of research has been carried out on various sensing techniques associated with the modification of an electrode based on nanocomposites and the correct immobilization of antibodies. Immobilization of affinity ligands and incorporation of an appropriate material in the transducer for enhanced signalling are the key attribute for developing an electrochemical sensor to overcome the limitations discussed above. This review describes the challenges and various strategies for signal amplification of sensors that lead to higher sensitivity *via* antibody immobilisation techniques and nanocomposite materials in electrochemical biosensor development.

Received 18th April 2022,
Accepted 23rd September 2022

DOI: 10.1039/d2ma00427e

rsc.li/materials-advances

1. Introduction

Due to their higher sensitivity and selectivity, electrochemical biosensors have recently emerged as a promising technique in the field of clinical diagnosis. They have also shown potential in developing a rapid detection system for early diagnosis of diseases.[1]

Department of Medical Devices, National Institute of Pharmaceutical Education and Research-Ahmedabad, Gujarat, India. E-mail: axay80@gmail.com, akshay.srivastava@niperahm.res.in; Tel: +91-9429371791
† Both the authors have equal contribution.

Mitkumar Patel

Mr. Mitkumar Patel received his master's degree in medical devices from National Institute of Pharmaceutical Education and Research, Ahmedabad, Gandhinagar, Gujarat. He has worked on developing electrochemical biosensors for early stage detection of chronic kidney disease (CKD). His research interests include electrochemical sensors, biomaterial based medical devices and biodegradable packaging solutions. He is currently developing environment friendly, scalable and commercializable biodegradable packaging solutions which are an alternative to the petroleum based packaging products.

Mayuri Agarwal

Mayuri Agrawal has received her Master's degree in Medical Devices from National Institute of Pharmaceutical Education and Research, Ahmedabad, Gujarat. She has worked in the field of diagnostics, developing biosensors with the potential to diagnose early-stage chronic kidney disease (CKD). Additionally, she has worked on a heart biosensor for constant monitoring of lipid profiles. She worked primarily with rapid, portable diagnostics.

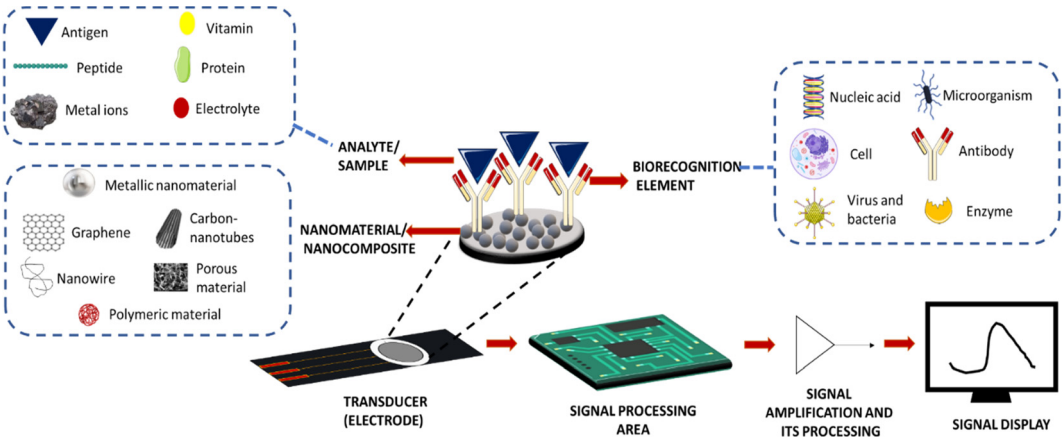

Fig. 1 Illustration of the components of an electrochemical immunosensor.

These electrochemical biosensors can help in monitoring biomolecules such as glucose, proteins, DNA, cholesterol, haemoglobin, *etc*. in body fluids.[2] Electrochemical sensors mainly consist of three parts: sample loading area, transducer area, and signal processing area[3] (Fig. 1).

The sample loading area is for keeping the analysing elements, and the electrode serves as a transducer in an electrochemical sensor. Typically, a transducer immobilises the biological recognition element. In an electrochemical sensor, when a specific analyte present in the sample binds to a biorecognition element attached to a transducer, it causes detectable changes in electrical characteristics such as potential differences in the electrical potential and conductivity. Conductometric, amperometric, and potentiometric measurements served as the foundation for these reactions. Electrochemical sensors are developed with higher sensitivity through the modification of an electrode made up of different materials. Working electrodes are generally composed of gold, platinum, or glassy carbon materials. Constant modifications of the working electrode using conducting materials and catalytic materials have been made to increase their sensitivity. A counter electrode is generally made of platinum due to its high conductivity. It can also stabilize the current with a working electrode. A reference electrode is made from saturated calomel or silver/silver chloride with a known electrode potential, which will help in measuring the potential of the working electrode during the reaction. In this review, we are focusing on how signal amplification strategies will impact the sensitivity of the electrochemical sensor and could also contribute to the early diagnosis of diseases by describing various antibody immobilization techniques and different nanomaterials used as substrates.

Signal amplification in electrochemical biosensors may also be useful for early-stage disease detection to improve the outcome of treatment. In nearly all cases, curative strategies do not succeed in preventing the disease progression to an irreversible stage due to a delay in the beginning of treatment as a consequence of a lack of early diagnosis. Medical diagnosis and further treatment decisions rely on the ability of diagnostic tests to identify and determine specific biomarkers in body fluids with high sensitivity and specificity. For the detection of diseases, various other types of techniques are also available, such as computed tomography (CT), fluoroscopy, low-dose CT, MRI (magnetic resonance imaging), and positron emission tomography (PET). These traditional diagnostic techniques have significant limitations, including radiation exposure, inability to be performed on a routine basis, high cost, limited accessibility in rural areas, and low sensitivity to disease diagnosis at an early stage.[4] On the other hand, immunoassay methods include fluorescence spectroscopy, chemiluminescence, radioimmunoassay, electrophoresis, polymerase chain reaction (PCR), and enzyme-linked immunosorbent assay (ELISA). They provide reliable results, but they also require expensive equipment, trained manpower, and appropriate labelling processes, and involve complex operating procedures.

On the other hand, the electrochemical point-of-care biosensor devices can be developed with higher sensitivity and specificity, which would allow faster, cost-effective, and non-invasive detection of a biomarker that may allow medical treatment at the initial stage. They will make results available to patients within a few minutes to improve their quality of life and provide better insight into the mechanistic basis of disease.

Akshay Srivastava

Associate Professor in the Department of Medical Devices at National Institute of Pharmaceutical Education and Research Ahmedabad, Gandhinagar, Gujarat. He has made significant contributions to the field of cell separation, biomaterials, and tissue engineering and medical devices. His research group is currently focusing on fabrication of biomaterial-based medical devices, bioconjugation of molecules, nanomaterials modifications, designing polymeric materials, biosensors and developing in vitro platforms to understand disease pathology.

An electrochemical immunosensor is a combined technology of electrochemical and immunoassay sensing. The electrochemical biosensors can also be explored for the early detection of a biological analyte in body fluids with higher sensitivity and by a faster signal amplification process.[5]

The materials as the electrode and supporting substrate have been involved in developing highly sensitive electrochemical biosensors since they provide the substrate for antibody immobilization and signal amplification. Despite the revolutionary changes that have been made in this sector, some challenges still remain in this field. The major challenge is the residence time of the sample with the transducer, which mostly affects the sensitivity. To tackle these problems, researchers are constantly trying to develop novel materials, such as a three-dimensional (3D) hydrogel system,[6] microfluidic chip integrated electrochemical biosensor,[7] aerogel modified electrode[8] and magneto immunosensor.[8,9] Ruiyi *et al.* developed graphene aerogel microspheres based on nanocomposites to capture specific cancer cells with high capture efficiency by increasing the residence time of the sample on a modified electrode.[8] The pH of the solutions also affects the sensitivity due to interference with the catalytic activity of nanocomposites and antibody–antigen reactions. It leads to changes in the amperometric response of the sensors.[10] A major problem faced by an enzymatic electrochemical sensor is the presence of a fouling agent and interference in the sample, which causes a reduction in amperometric signals. Sometimes changes in pH and chemical composition of body fluids due to pathological conditions and altered enzyme activity also cause interference in detection.[11] In the current scenario, electrochemical immunosensors mainly suffer from – poor reproducibility and sensitivity. The main concern is the optimum accessibility of the antibody, which solely depends upon the immobilization method and substrate sensitivity. The conventional method of antibody immobilization usually leads to random, non-reproducible, and less sensitive measurements, whereas novel site-directed approaches increase sensitivity. Other concerns compromising the sensitivity include heterogeneous surface coating, which leads to complications in antibody immobilization contributing to inaccuracy, false positive and negative results, lack of reproducibility, and random immobilization of antibodies.[12] Sample preparation, detection time, and real-time sensing are some of the major limitations for detection. Besides all these challenges, developing a mathematical model for a multi-analyte detection system by using a computational approach is another challenge that needs to be addressed.[13] The microarray platforms have also been developed for the fully automated determination of specific markers.

In the past decade, several studies have been conducted and reviewed on the development of novel strategies for signal amplification by using nanomaterials and conjugated biomolecules.[14] There is also a brief explanation of methods for functionalizing nanomaterials and how they might help with biosensing[15] and how nanoparticles may be used to make electrochemical sensors.[16] However, our article will outline current developments and a technique for making electrochemical biosensors. In the following sections, we have discussed various strategies for controlling the orientation of antibody conjugation and different nanomaterials to enhance signal amplification in developing electrochemical biosensors. This review combines several reviews to provide the readers with a comprehensive notion of research in one review.

2. Signal amplification strategies in electrochemical biosensors

2.1. Antibody immobilization strategies

To attain a fully functional and effective antibody after conjugation, the conformation of antibodies should not be affected, especially at their active site. The sensitivity of an electrochemical immunosensor mainly hinges on the antibody–antigen reaction, which is critical for analyte detection. Antibodies consist of two fragments: (i) antigen-binding region (Fab) and (ii) crystallizable (Fc) region. The variable domain (Fv) at the N-terminus is localized in the Fab region, which is an antigen-binding site that contains 110 residues of amino acids. The functional group on the substrate can be conjugated with the functional groups present on antibodies, such as amino groups in the lysine residue, thiol groups in the cysteine residue, and aldehyde groups generated by the oxidation of carbohydrate residues in the Fc portion of antibodies. Various antibody immobilization methods have been applied and recently reviewed elsewhere.[17] It is important to consider that the immobilized antibodies should not be masked, since they indirectly amplify the signal and contribute to better sensitivity.[18,19] Site-specific covalent binding of an antibody to a transducer is essential not only for good sensitivity but also for reproducibility. In the following sections, we have covered several strategies for antibody immobilization, which have shown their application in developing electrochemical sensors. This will eventually assist readers to overcome challenges while developing electrochemical biosensors with high sensitivity.

2.1.1. Random immobilization

(A) Non-covalent immobilization. Non-covalent immobilization is a simple and cost-effective immobilization technique based on electrostatic, ionic, entrapment, hydrophobic, hydrophilic and van der Waals forces between proteins and substrates but often leads to weaker, random immobilization and denaturation of antibodies eventually giving poor reproducibility[19,20] (Fig. 2). Random immobilization lowers active site accessibility due to steric hindrance. The impact of pH on the orientation of antibodies physically adsorbed onto gold nanoparticles *via* electrostatic interactions was also investigated. It was found that as the pH was decreased, the accessibility of the antigen-binding site (Fab) increased.[21] The reason behind it was that as the pH varied, the surface charge distribution on the antibodies modulated as well. It is also reported that maximum adsorption occurs at pH near or above the isoelectric point.[22] The physical adsorption method is often weak, and is sensitive to pH, temperature, salt concentration, and isoelectric point of the antibody leading to poor analytical performance and low operational and storage stability. More often, PEG (polyethylene glycol) or BSA (bovine serum albumin) is added

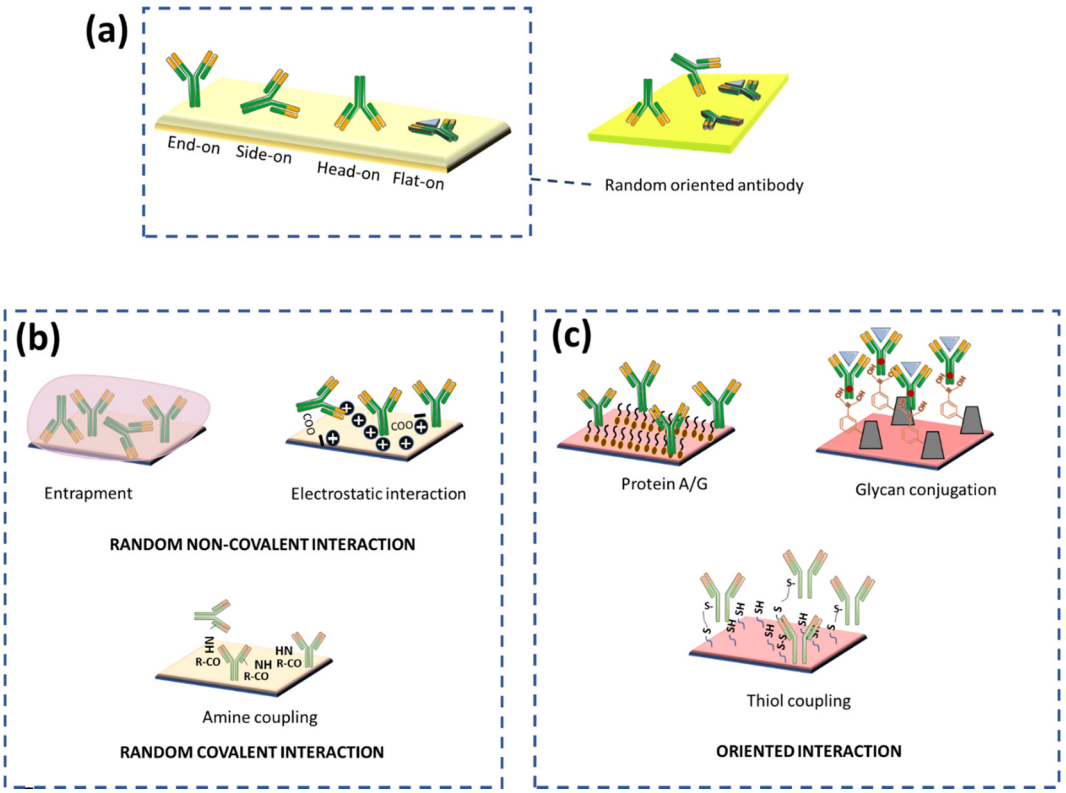

Fig. 2 (a) Possible orientation of antibody immobilization on the surface, (b) random immobilization methods, and (c) correctly oriented immobilization methods.

to block the remaining free conjugation sites on gold nanoparticles and prevent nonspecific binding to minimize nonspecific binding.[21,22] In an interesting example of early diagnosis, a highly sensitive, cost-effective and user-friendly ZIKV immunesensing chip for early detection of the zika virus was developed. The interdigitated microelectrode of the gold (IDE-Au) chip was functionalized with dithiobis succinimidyl propionate (DTSP) for physical immobilization of the ZIKA-envelope protein antibody (Zev-Abs). The antibody was immobilized *via* electrostatic interaction on the IDE-Au chip. The linear range was found to be 1 pM to 10 pM and the LOD (limit of detection) was 10 pM.[23] In some cases, the targeted protein was passively adsorbed on the working electrode and gold nanoparticles were used as a labelling agent on which antibodies were immobilized *via* ionic and hydrophobic interactions. A signal is generated when colloidal gold is oxidized and gives $AuCl_4^-$ ions which can be determined *via* adsorptive voltammetry. Within the range of 10 to 500 ng mL^{-1}, a linear relationship between antigen concentration and wave amplitude was discovered, with a LOD (limit of detection) of 4 ng mL^{-1}.[24] Nevertheless, this category of methods is time-consuming, and highly unstable for the regeneration (analyte removal from the antibody) of the antibody due to the weaker interaction of antibodies with the substrate surface.[25] Another approach for physical adsorption uses entrapment within the gel or polymer; this may include hydrogels which will contribute to increasing the surface area because of their porous nature. Covalent bonding is more stable and effective; however, it is also claimed that antibody immobilization on nanomaterials based on the adsorption method is more effective than that based on covalent bonding.[26]

(B) Covalent immobilization. Covalent immobilization is a highly stable method to immobilize antibodies but the choice of method depends upon the stability of the antibody. The covalent antibody conjugation method requires the presence of mutually reactive groups on the substrate and antibody. Primary amines in the lysine amino acid, carboxylic acid in glutamic and aspartic acid, thiol in cysteine, hydroxyl in serine and threonine, phenol in tyrosine, thioether in methionine, imidazole in histidine, and guanidino in arginine are the reactive groups on antibodies. Correspondingly, the substrate should also be functionalized with various groups like amino, carboxyl, and sulfhydryl for the conjugation. Shen *et al.* have fabricated a simple, sensitive, and effective thiol aromatic aldehyde (TAA)-based electrochemical immunosensor for antibody immobilization. A novel sulphur-containing linker with an aldehyde group on the substrate was synthesized which can form a covalent bond with an amino group of antibodies without any additional chemical crosslinking step. The developed immunosensor was used to detect IgG in the patient samples. The linear range was found to be 0.01 to 25 ng mL^{-1} with an LOD of 0.003 ng mL^{-1}.[27] Furthermore, the covalent immobilization method yields better reproducibility compared to physical adsorption. Chen and colleagues demonstrated a

physical adsorption method for conjugation of antibodies on gold nanoparticles *via* hydrophobic interaction, but the developed immunosensor showed low sensitivity (LOD of 4 ng mL^{-1}).[24] Despite the fact that covalent bonding promotes stable immobilisation of antibodies, it results in disordered antibody orientation due to the loss of binding capacity. The major factor for the decrease in binding capacity is the random orientation of antibody molecules and steric hindrance on the surface of the substrate. Antibodies containing amino groups and –COOH groups can be targeted *via* carbodiimide (EDC) in combination with *N*-hydroxy succinimide (NHS) for covalent bonding between the carboxylated substrate and the antibody. The distribution of amine and carboxyl groups on antibodies governs random interaction with the substrate *via* the formation of an amide linkage. Nawaz *et al.* have utilized EDC/NHS-based conjugation chemistry for the fabrication of disposable electrochemical immunosensors for early diagnosis of dengue. A screen-printed electrode (SPE) was electro-grafted with BSA before immobilisation to increase antifouling and conductivity properties. The carboxylic groups of BSA were then activated *via* EDC-NHS and the antibody was immobilized *via* the formation of an amide linkage. The LOD of the developed sensor was found to be 0.3 ng mL^{-1} and the linear range was 1–200 ng mL^{-1}.[28] Raghav *et al.* compared three different antibody immobilization strategies for the detection of ovarian carcinoma antigen CA125, *i.e.*, the EDC/NHS strategy, direct immobilization on citrated gold NPs, and direct immobilization on L-asparagine functionalized gold NPs (Asn-AuNPs). It was found that direct immobilization on Asn-AuNPs demonstrated 2.5 times more sensitivity compared to the EDC-NHS strategy and 2 times more sensitivity than direct immobilization on citrated gold NPs. One of the reasons behind the low sensitivity of EDC/NHS is the presence of a large number of amine groups on antibodies, which causes random immobilization leading to difficulty in the binding of CA125 to the antibody epitope. On the other hand, Asn-AuNPs contain both–NH_3^+ and COO^- groups on their surface, which can control the immobilization of the Fc region and the R group of antibodies. The linear range of sensitivity for the EDC/NHS strategy was found to be 0–50 IU mL^{-1} and for direct immobilization on L-asparagine functionalized gold NPs (Asn-AuNPs) it was 0–100 IU mL^{-1}.[29] A well-known and less time-consuming method relies on the direct immobilisation of the target analyte on the substrate, which is made feasible by the bioactivity or affinity of proteins that are attached to surfaces.[30] Researchers have also been employing direct miRNA immobilisation on gold-loaded superparamagnetic ferric oxide nanocubes, allowing methylene blue (MB) to attach to the negatively charged phosphate backbone of adsorbed miRNA. Then this will induce a redox reaction leading to charge generation as a function of time. The amount of charge generation is proportional to MB, and MB is a direct function of miRNA concentration.[31] Md. Nazmul Islam and colleagues used gold-loaded nanoporous superparamagnetic iron oxide nanocubes (Au@NPFe_2O_3NC) to detect microRNA at the attomolar level. Nanocubes allows direct adsorptive attachment of miRNA to the surface of Au@NPFe_2O_3NC. The cationic RuHex was electrostatically coupled with the surface-attached anionic phosphate backbone of the miRNA and was measured *via* chronocoulometric (CC) charge detection. The test demonstrated remarkable repeatability (percent RSD <= 5 percent, for $n = 3$) and allowed for an extremely low level of detection of 100 aM.[32]

Covalent immobilization strategies are specific to a specific group, but still they are not completely selective, *e.g.*, amino coupling results in random immobilization as seen in the above example due to the availability of amino groups all over the surface of the antibodies. However, this random immobilization can be somehow minimized *via* site-specific antibody modification by using the principles of genetic engineering, or a specific chemical tag. Genetic engineering is used to create monovalent and multivalent fragments. These antibody derivatives are legitimate alternatives to full-size mAbs because they retain the targeting specificity while being synthesized more cost-effectively by using recombinant DNA technology principles. Antigen-binding (Fab) fragments, single-chain variable fragments (scFv), diabody, mini body, and variable domains produced from heavy chain-only antibodies (VHH) are some examples. The modified antibody contains an amino or carboxyl group at a specific location, allowing for oriented immobilisation on the surface of the electrodes. Alternatively, the fragmented antibody can be tagged with an amine-rich patch of lysine (poly(lysine) tag) or the sulfhydryl groups present at the hinge region in an oxidized form as disulfide bonds. These bonds can be selectively broken using reducing agents to provide free sulfhydryl groups, which can be conjugated to the substrate through different cross-linkers, achieving oriented immobilization.[33] To break the disulfide bonds, various reducing agents such as monothiol,[34] dithiol,[34] 2-mercaptoethylamine hydrochloride (2-MEA),[35] and tris(2-carboxyethyl)phosphine hydrochloride[36] are used. The mechanism is the bonding of the thiol group of monovalent antigen-binding Fab fragments to hydrophilic gold as a substrate or any other substrate having a thiol group *via* a self-assembly process. Arkady A. Karyakin and co-workers demonstrated that half thiol-modified IgG antibodies conjugated on a gold substrate promote higher binding of antibodies with better sensitivity.[37]

2.1.2. Site oriented binding strategies. Site-oriented antibody binding strategies have been employed to improve the sensitivity of electrochemical immunosensors. The most fundamental and significant benefit of site-directed conjugation is the increase in antigen-binding capacity up to 2 to 8 times, which results in better sensitivity and stability in various biomarker detection. Targeting several functional groups present on antibodies, such as the sulfhydryl group, carbohydrate group oxidation (glycan conjugation), and immobilisation *via* the nucleotide-binding site (NBS) can result in site-directed immobilisation of antibodies. It is well reported that the NBS is a highly conserved area between the variable regions of light and heavy chains of the Fab domains of all the antibodies having affinity towards IBA (indole-3-butyric acid). It has been demonstrated that this unique site-specific binding strategy *via* crosslinking IBA to an NBS using ultraviolet radiation (254 nm) without affecting the structural and functional parts of the antibody can provide higher sensitivity. IBA (indole-3-butyric acid) can form covalent bonds with NBS due to the generation of active radicals in the aromatic rings of both IBA and NBS in the presence of UV radiation.

Furthermore, IBA can be attached to a solid substrate by tagging IBA with thiol, biotin, and fluorescein, which can couple with the sulphide group, streptavidin, and maleimide, respectively.[38,39] Other approaches for site-directed immobilization are *via* protein A/G, where the cell-wall proteins found in *Staphylococcus aureus* and *Streptococcus* species bind specifically to the Fc portion of antibodies. Other methods include affinity interaction, self-assembled monolayer (SAM) technique,[40] "click" chemistry, biotin–streptavidin interaction,[41] nickel-nitrilotriacetic acid and 6-histidine interaction (Ni-NTA-His). Moreover, antibodies having specific binding affinity for materials can be developed for the easy immobilization on the biosensor devices.[42] Other affinity ligands such as aptamers, peptides, half-sized antibody, ScAb, ScFv, Fab, F(Ab)2, Fab′, F(Ab′)2, and nanobody have also been recently explored for biosensor applications (Fig. 2).[42]

Site-directed conjugation can be achieved by covalent as well as non-covalent bonding. The Ab fragment can be changed by incorporating positively charged amino acids (arginine) in the peptide linker or a 6-histidine amino acid sequence in the C-terminus for immobilisation *via* electrostatic and non-covalent bonding. The bio-affinity approach may also be used to immobilise scFv on streptavidin-coated surfaces by conjugating to biotin through free amines on the scFv. Antibodies are also covalently immobilized *via* bioorthogonal chemistry, and the click reaction plays a critical part in achieving this since it is an efficient and highly selective reaction. A 'click' reaction is defined by its mild reaction conditions, lack of sensitivity to oxygen and water and production of a stable product under physiological conditions. Click reactions include copper or ring-strain catalyzed azide–alkyne cycloaddition, production of oxime, Diels–Alder cycloaddition, Staudinger-ligations, thiolene additions, *etc.*[43] An engineered antibody fragment for covalent bonding is another approach where the engineered antibody's cysteine (free thiol group) residue can be introduced to form covalent bonding with all the advantages of engineered antibodies and covalent bonding. The interference of contaminants on the surface of the sensor is reduced because of the homogeneous characteristics of the scFv in comparison to a complete antibody or Fab fragment. The position of the free cysteine within an scFv has a significant impact on the production level of an antibody in *E. coli*; thus, the position of cysteine is placed within areas that have less impact on protein folding, like the linker sequence. Highly stable coupling can withstand higher flow rates and harsh conditions and hence can be used for regeneration purposes as well.[25,44]

Another approach to the site-directed orientation is the utilization of the carbohydrate group present in the Fc region of antibodies. The *cis*-diol groups of sugar can be transferred to the aldehyde using periodate oxidation, which can further react with hydrazide or amino groups. This group can also be targeted *via* boronic acid-modified substrates because boronic acid forms a cyclic boronate ester with vicinal diols present in the Fc region of antibodies (Fig. 2). Thus, it provides oriented binding of antibodies on a substrate.[20]

Other intriguing protein ligands include protein A and protein G, which have 5 and 3 affinity binding sites for IgG, respectively. Interestingly, the binding affinity is towards the Fc region (nonantigenic) of IgG, which leads to oriented immobilization with minimum steric hindrance. Sanchez-Tirado and co-workers developed an electrochemical immunosensor for the determination of TGF-beta 1 cytokine using an antibody-conjugated protein A ligand. The magnetic nanoparticle nanocomposite was prepared and the immobilization of the antibody was carried out. It was demonstrated that the protein A ligand-based antibody binding strategy increases the sensitivity of the developed immunosensor. The developed immunosensor showed a linear response from 5 to 200 pg mL^{-1} and the limit of detection was 1.3 pg mL^{-1}.[45] Yao *et al.* reported an electrochemical impedimetric sensor for detection of the same antigen (TGF-beta 1) but it exhibited a lower sensitivity (LOD of 0.570 ng mL^{-1}) than the previously developed sensor by Sanchez-Tirado *et al.* The reasons behind the lower detection limit could be attributed to the used bare inter-digitated gold electrode and antibodies conjugated *via* covalent bonding, which leads to random orientation of antibodies and thus lower sensitivity.[46] Afsharan *et al.* used biotin-streptavidin interaction to immobilize antibodies in the correct orientation for the detection of the p53 protein. The glassy carbon electrode was modified with thiolated graphene oxide (t-go) which contributes to higher conductivity and interaction with streptavidin-modified gold nanoparticles (Str-Au NPs). A higher amount of biotinylated p53-antibody was conjugated to the composite due to its higher surface area. The electrochemical immunosensor demonstrated a linear range from 2 to 200 pM and the LOD was about 30 fM. The reason behind ultrasensitive detection can be attributed to modified graphene and gold particles because they increase electron transfer rates and capture antibodies.[47]

Luo *et al.* developed a disposable electrochemical immunosensor for the detection of p53. As a signal amplification strategy, sandwich-type immunoreactions were utilized, where carbon nanospheres functionalized with an enzyme were used as a label and magnetic beads were utilized as an electrochemical transducer. Magnetic beads were conjugated with primary antibodies *via* the EDC-NHS crosslink strategy. Magnetic beads provide a higher surface area to capture antibodies. The EDC-NHS strategy leads to random orientation of antibodies, which negatively impacts the sensitivity of the immunosensor. In this sensor, the limit of detection was found to be 3.3 pg mL^{-1}, demonstrating that this sensor is not as sensitive as the previously developed p53 sensor. In another study, deposition of gold nanoparticles onto a screen-printed graphite (SPGE) electrode followed by adsorption of monovalent half-antibody (monoAb) fragments of the anti-biotin antibody *via* Au–thiol bonds (monoAb/AuNP/SPGE) was carried out.[38,48] Similarly, the interaction of boronic acid and sugar moieties present on the anti-biotin antibody was utilized by developing a boronic acid-coated screen-printed graphite-electrode (SPGE) surface. It was found that despite having a higher density of antibodies for monoAb/AuNP/SPGE (*i.e.*, five times more than that of the Ab/APBA/SPGE biosensor), the sensitivity of the Ab/APBA/SPGE biosensor (0.19 pg) was 250 times more than that of the monoAb/AuNP/SPGE system (50 pg). This is due to the Ab/APBA/SPGE biosensor

Table 1 Summary of site directed antibody immobilization techniques with their key points

Sr. No	Type of immobilization	Functional group	Description	LOD and linear range	Comments	Ref
1.	Biochemical or bioaffinity	Protein A/G	Detection of cancer using EGFR biomarker in brain tissue and human plasma	LOD – 0.34 pg mL^{-1} Linear range – 1 pg mL^{-1} to 1 μg mL^{-1}	• Site-directed orientation of antibodies • Antigen-binding ability is increased by 2–8 times • Lowers the limit of detection, enhances sensitivity, and expands the dynamic range of the sensor • Decreases steric hindrance	50
		Z-domain or ZZ protein or ZZ-BNC(engineered) bionanocapsule with Z domain	Leptin based biosensor for obesity disease	LOD – 0.00087 pg mL^{-1} Linear range – 0.001 to 1000 pg mL^{-1}	• These are engineered analogs having the specific monovalent binding site to the Fc part of the antibody • Oriented immobilization with high sensitivity • Real-time analyses of antibodies possible	40 and 51
		Biotin and streptavidin or avidin	Detection of ovarian cancer using carbohydrate antigen 125	2 linear ranges – 0.001–0.1 and 0.1–30 ng mL^{-1}; LOD – 0.5 pg mL^{-1}	• Biotin–streptavidin sort of interaction can provide high sensitivity and specificity • One of these moieties is linked to a substrate and another one to the antibody • These interaction remain unaffected by pH, temp, solvent, or denaturation agent • Strongest known non-covalent coupling and biological interaction with a dissociation constant of 1015 M	52
		Polyhistidine tag having affinity for Ni-NTA surface	Detection of insulin concentration	10 pM–100 nM	Polyhistidine tag make coordination complex with metal ions (Cu^{2+}, Zn^{2+}, Ni^{2+} *etc.*). • $(His)_6$ is linked to the desired antibody	53
2.	Recombinant antibodies	Single chain antibodies (ScAb)	Detection of prostate cancer	Sensitivity – 0.5 ng mL^{-1} Linear range up to 10 ng mL^{-1}	• Smaller size, high-density immobilization, high sensitivity, stability and easy genetic manipulation • Suitable for bioconjugation to nanoparticles • When compared to single-chain fragment variable (scFv) antibody derivatives, the ScAb constant domain (Ck) provides better-oriented immobilisation (through amino groups) • Compared to other recombinant antibody formats, ScAb exhibits higher levels of expression in *E. coli*	54 and 55
3.		Single chain Fv (ScFv)	Detection of cocaine	Linearity 5.0 and 250 ng mL^{-1} LOD – 3.6 ng mL^{-1}	• ScFV contains light and heavy chain domains that are connected by a flexible peptide connector • Antibody fragments outperform full antibodies in terms of customizability, surface densities, and immobilization choices, and are 35 times more active than complete antibodies due to their smaller size • Hex histidine tags, cysteine residues, polystyrene-binding peptides, biotins, and Cys3-tags can all be added to recombinant scFv fragments	56
4.		F(ab′)2	Insulin detection	100 ng mL^{-1} to 100 g mL^{-1}	• Generated by digesting entire antibodies with pepsin while leaving the hinge region intact. It is divalent, having an MW of 110 kDa, and comprised of two antigen-binding F(ab) sections joined together by disulfide bonds • It is sometimes used to obtain Fab′, *i.e.* after reducing F(ab′)2, Fab′ is obtained	57
5.		Nanobody (only Vh or Vl domain)	Detection of AFB1 through AFB1-HCR as a signal amplifier	LOD – 68 fg mL^{-1} Linear 0.5 to 10 ng mL^{-1}	• Significant due to its small size (12–15 kDa) and increased thermostability in comparison to scFv domains • Antigen binding at nanomolar affinity • It has limited applications due to poor functional yields	58
6.		Fab	Detection of *Francisella tularensis*	LOD – 4.5 ng mL^{-1} for the lipopolysaccharide antigen, 31 bacteria mL^{-1} for *F. tularensis*	• Generally obtained after papain digestion • Fab is comprised of heavy and light chains each having one constant and one variable	59

Table 1 (*continued*)

Sr. No	Type of immobilization	Functional group	Description	LOD and linear range	Comments	Ref
					domain, with the variable domain serving as an antigen-binding site • They are without sulphide bond • They are cost-effective compared to ScFv fragments • Fab′ is obtained after reducing F(ab)2	
	DNA directed immobilization (DDI)	DNA can act as a linker	*E. coli* O157:H7 detection	f 48 colony-forming unit (CFU per mL)	• A solid support is modified with a single strand (SS) nucleotide which is complementary to the strand present on an antibody	60
				Dynamic range (up to 107 CFU per mL)	• Sometimes instead of linking SS to antibody, it is linked to protein G, inculcating strengths of both protein A and DDI as well using such a method no additional antibody modification is needed • Possibility of regeneration of surface by denaturation of DNA • The demerit of DDI is that DDI replaces site-directed protein attachment on the support surface with site-selective oligonucleotide-protein conjugation • Multi-step processes are needed, hence increasing cost and time	
		Fc portion glycan moiety	Lymphoma cancer cell detection	100–1 000 000 cells per mL	Fc portion consists of carbohydrate/glycan, this glycan has selectivity and affinity towards lectin, Fbs1 complex and boronic acid can react with diols forming a reversible cyclic boronate bond, making it a good candidate for producing a reversible biosensor	61
				LOD – 38 cells per mL	Using glycan one can achieve highly selective and site-directed antibody immobilization Without a spacer, it may become inaccessible after immobilization. Site-directed immobilization can be achieved by using boronic acid-modified nanomaterials	

having site-directed orientation of the antibody based on the boronic acid strategy for immobilization; the surface had a minimal but adequate number of antibody binding sites, which eventually led to the monoAb/AuNP/SPGE system (50 pg). This is due to the Ab/APBA/SPGE biosensor having site directed orientation of the antibody using the boronic acid strategy for immobilization; the surface had a minimal but adequate number of antibody binding sites, which eventually led to an improved limit of detection.[49] In Table 1, we have summarized various novel antibody immobilization techniques for site-directed conjugation.

3. Nanomaterials for modification of the transducer towards higher precision and sensitivity

Nanomaterials have a vital role in signal amplification due to their controllable small size and quantum effects, which help in enhancing signals when present in direct contact with the biorecognition element that interacts with the analyte of interest.[62] These nanomaterials, along with the correctly oriented antibody conjugation on their surface, directly impact the sensitivity and reproducibility. Nanomaterials conjugated with antibodies provide an interface for sensing physical changes caused by biochemical interactions and converting this input into detectable signals by increasing the current yield.[63] Donghai Lin and colleagues revealed that conjugation methods for producing oriented antibodies improve sensitivity. However, when similar methods are applied to nanoparticles, they provide a synergistic effect toward increasing sensitivity.[64] Due to their unique chemical and electrical characteristics, nanomaterials can also contribute to the development of innovative and enhanced sensing devices with higher sensitivity and specificity. Several nanomaterials have been studied as transducer materials, such as metals, carbon materials, polymeric nanocomposites, semiconducting materials, and molecular imprinted polymers, which are discussed in the following sections.

3.1. Metal-based nanomaterials

Metals are among the most elegant signal amplification materials utilized in electrochemical biosensors. Metallic nanomaterials act as an ideal transducer platform to increase the active surface area because of their small size and large surface area. The small size and large surface area of metal nanoparticles provide excellent conductivity by facilitating direct electron transfer between

biomolecules and electrode surfaces. In electrochemical biosensors, both noble and non-noble metal nanoparticles are utilized as transducers and are discussed in the following sections.[65,66]

3.1.1. Noble metal-based electrochemical biosensors. The primary roles of metal nanoparticles (MNP) are immobilization of biorecognition elements, mediating electron transfer by acting as an electron wire which permits electron transport from the bioreaction where it is produced to the sensing electrode, catalyzing bioreactions with their substrate, amplifying mass change, and enhancing refractive index changes.[67] Noble metal-based nanoparticles have distinctive features like plasmonic activity, high conductivity, large surface area, and electrocatalytic activity. Noble metals provide an oxide-free surface, making it easier for the conjugation of biorecognition elements. These materials also demonstrate size-dependent electromagnetic and chemical activity.[68] Noble metals such as ruthenium (Ru), rhodium (Rh), palladium (Pd), silver (Ag), platinum (Pt), and gold have been investigated in various signal amplification schemes (Au) in electrochemical biosensors. Furthermore, the size and form of nanoparticles have a significant impact on these capabilities. Changes in the form can affect the properties of nanomaterials such as surface atom coverage and electrocatalytic activity, potentially leading to increased activity.[69] Gold nanoparticles (AuNPs) are promising nanomaterials that have opened up new possibilities for the development of sensitive electrochemical biosensors. AuNPs have several distinct characteristics, including ease of preparation, good biocompatibility, higher conductivity, unique electrical properties, and a large surface area-to-volume ratio. Furthermore, electrodes treated with gold nanoparticles showed a nearly three-fold increase in electroactive area, resulting in a larger functional density of biomolecules and simpler electron exchange.

The bottleneck of an electrochemical biosensor is the need for highly specific chemical probes that will specifically bind to the analyte of interest because any undesired molecule present in the complex sample could bind to the electrode and decrease the current density, which will eventually decrease the sensitivity of the sensor. Recently, researchers have developed an antifouling coating electrode having a 3D porous matrix of cross-linked bovine serum albumin (BSA) using glutaraldehyde supported by gold nanomaterial. These modified electrode coatings preserved 88% of the original signals even after 1 month of exposure to unprocessed human plasma, and immobilizing specific antibodies allowed detection of IL-6 with higher sensitivity.[70] Another challenging application is the detection of alpha-fetoprotein (AFP) which is a cancer biomarker that can be detected at an early stage by using highly sensitive electrochemical immunosensors.[71] The normal concentration of alpha-fetoprotein in humans is 10 ng mL^{-1}, but it deviates significantly from normal concentrations in fatal liver injury, liver carcinoma, and gastrointestinal tumours.[72,73] Jantima Upan with other colleagues reported an electrochemical immunosensor for early detection of cancer using AFP as a biomarker. They demonstrated that platinum nanomaterials decorated on the carboxylated graphene oxide coated screen-printed graphene- carbon paste electrode (SPGE) could enhance the sensitivity. The developed sensor had a linear range of about 3.0–30 ng m^{-1} with a LOD of about 1.22 ng m^{-1}.[74] A worm-like platinum nanomaterial-based highly sensitive sensor was also developed for the determination of ALP. The sensor had a wide linear dynamic range (0.0001–100 ng mL^{-1}) and a LOD of about 0.028 pg mL^{-1}.[75] In a separate example, it was shown that cobalt oxide possesses distinctive intrinsic peroxidase-like activity and demonstrates better stability at higher H_2O_2 concentrations than horseradish peroxidase (HRP).[76] Liu *et al.* prepared a Co_3O_4/graphene nanocomposite material to achieve higher electrical activity. The incorporation of nanoparticles in graphene matrix provides a higher surface area, which makes it a suitable matrix for loading noble metals (Pt-NP) with higher catalytic activity and increased electrical properties. FTIR spectra indicate a successful combination of 3-mercaptopropyl triethoxysilane (MPTS) and graphene sheets (GS) (Fig. 3A). SEM images have shown the particle nature of Co_3O_4 and Pt NPs incorporated into graphene material (Fig. 3E). The EDS image indicates the presence of carbon dioxide and an oxygen element proving that Co_3O_4/graphene was synthesized (Fig. 3F). The developed material was fabricated in the form of a transducer in an electrochemical immunosensor (Fig. 4). The linear range was found to be 0.1 pg mL^{-1} to 60 ng mL^{-1} and the LOD was 0.029 pg mL^{-1}.[77] Furthermore, metal-binding cysteine (Cys) or histidine (His) amino acids in the peptide linker are tailored to improve antibody conjugation on metal surfaces in an oriented manner and allow appropriate self-assembly on metal surfaces. Researchers fabricated a fluorine-doped tin oxide electrode, modified it with Au nanoparticles, and on this surface, SARS-CoV-2 Spike S1 antibody was immobilized. The response was measured using CV and DPV. The LOD was about 0.63 fM in standard buffer and 120 fM in spiked saliva samples with negligible cross reactivity with the Middle East Respiratory Syndrome (MERS) spike protein.[78]

3.1.2. Bimetallic nanoparticles for signal amplification. Bimetallic materials are characterised by the formation of intermetallic bonds, which allow intermetallic charge transfer, as well as changes in particle size and morphology. Bimetallic materials demonstrate abundant catalytic and electrical capabilities, and have recently attracted a lot of attention in developing a bimetallic-based signal amplification matrix. Min Hu *et al.* fabricated a cobalt–nickel bimetallic organic framework immobilized on a gold electrode for the detection of miRNA 126 *via* immobilization of the complementary DNA onto the modified electrode. The sensor had an ultra-low LOD, which was about 0.14 fM. This strategy also showed promising results for the detection of cancer biomarkers, and could be used for fabricating different biosensors with different targets.[79] In another report, novel mesoporous bimetallic films of the gold (Au) and silver (Ag) alloy were prepared by electrodeposition. The developed electrode showed enhanced signal amplification with increased miRNA adsorption sites. It showed enhanced catalytic activity and sensitivity for single step rapid detection of miRNA.[66] Palladium–silver (Pd Ag) nanoparticles with carbon paste-based electrodes were reported for developing an ultrasensitive electrochemical sensor for the detection of uric acid. High-angle annular dark-field scanning transmission

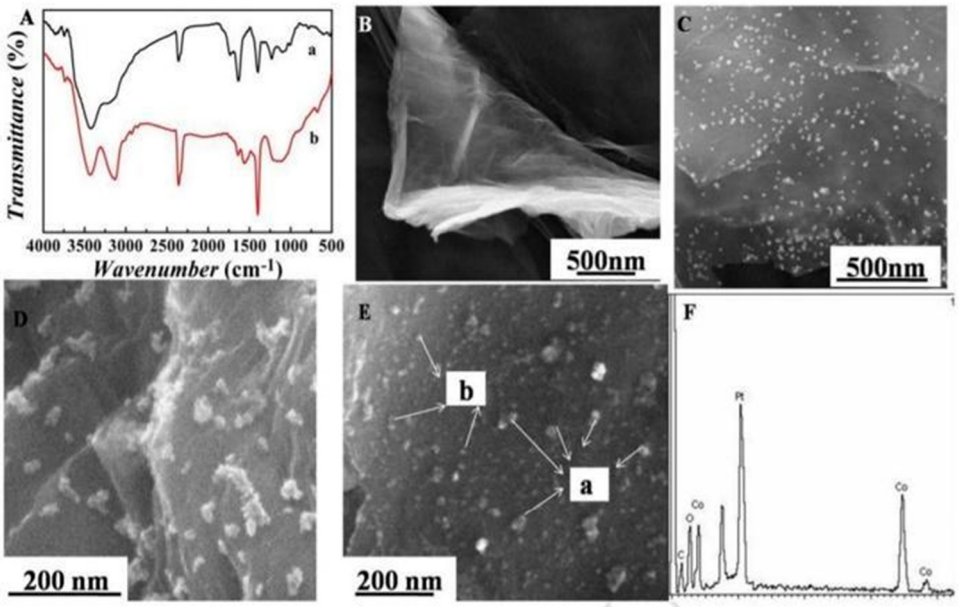

Fig. 3 (A) FT-IR spectrum of GO (a) and MPTES-GS (b); (B) SEM image of GO; (C) SEM image of Au@MPTES-GS; (D) SEM image of Co_3O_4/graphene; (E) SEM image of Pt NPs/Co_3O_4/graphene: (a) Co_3O_4, (b) Pt NPs; and (F) EDS spectrum of Pt NPs/Co_3O_4/graphene. Reproduced from Liu *et al.* (2017).[77]

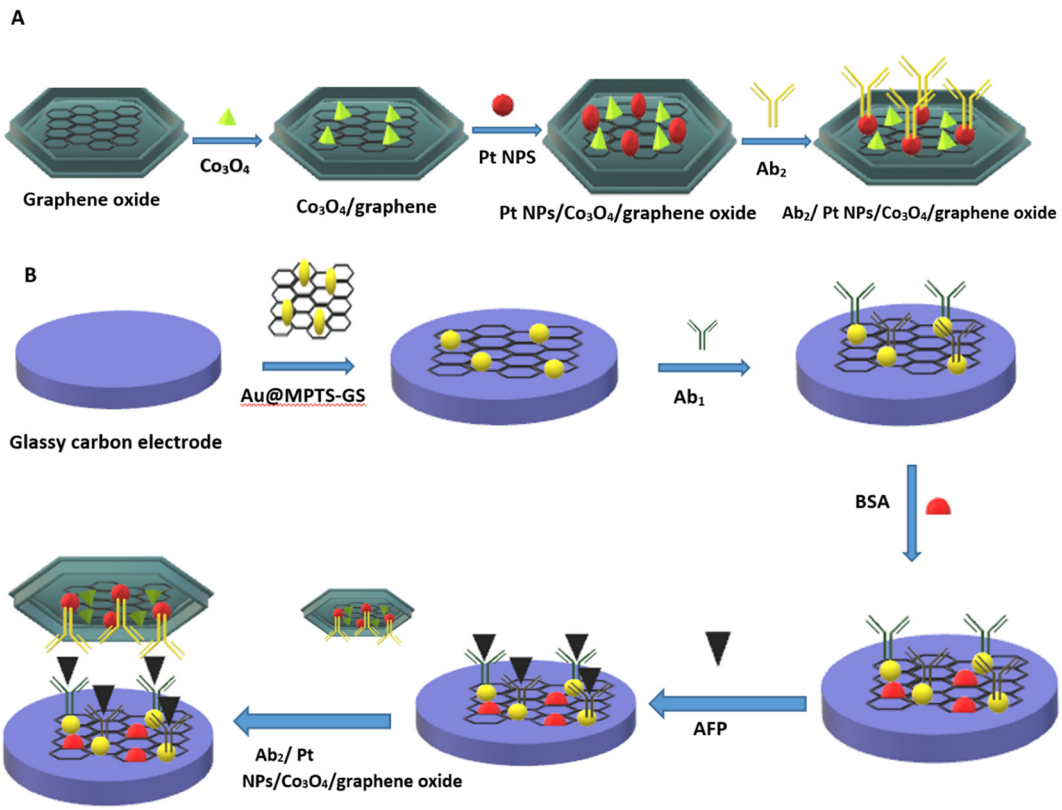

Fig. 4 (A) Alloy matrix nanocomposite of transition metal oxide (cobalt oxide (Co_3O_4)) and noble metal nanoparticle (platinum nanoparticle (Pt-NP)). (B) Schematic representation of fabrication of a sandwich-type electrochemical immunosensor. Redrawn with modification from Liu *et al.* (2017).[77]

electron microscopy (HAADF-STEM) analysis revealed the size of the nanoparticles as about 10 nm and thus having a higher surface to volume ratio. The small size and high surface area of bimetallic nanoparticles are mainly responsible for the higher

catalytic performance of developed bimetallic nanocomposites. The electro-catalytic activity of the nanocomposite was assessed by cyclic voltammetry (CV) and differential pulse voltammetry (DPV). The LOD and quantification limit were found to be 5.543 nM and 16.64 nM, respectively. The linear range was also obtained as 4.69–273 nM.[80] The bimetallic material has a role in increasing the current response as well as a vital role in the catalysis of methylene blue reduction which directly contributes to amplifying the response. Zheng *et al.* (Fig. 5) fabricated an electrochemical biosensor for the detection of prostate-specific antigen (PSA) using AuPt bimetallic material. The peptide having an affinity for PSA was captured on the surface of the modified electrode functionalized with methylene blue. The redox signals generated by methylene blue demonstrated a LOD of about 16.7 fg mL^{-1} and a linear dynamic range of 0.00005–10 ng mL^{-1}.[81] In some sensors, bimetallic nanoparticles were also used with support materials like carbon nanotubes, graphene, and silica derivatives.[82]

An ultrasensitive sandwich-type electrochemical immunosensor for prostate cancer was also developed using a platinum-copper-based nanomaterial. Higher signal amplification was obtained by using a bimetallic nanocomposite made of PtCu hybrid nanomaterials. Pt has super catalytic activity against H_2O_2, and Cu nanoparticles possess a catalytic effect. 2D/2D rGO/g-C_3N_4 sheets were used to overcome the limitations of nanoscale particles because these sheets provide a large surface area with excellent conductivity and good thermal-chemical stability. To overcome the poor conductivity of g-C_3N_4, 2D rGO was incorporated for better electrical conductivity with efficient charge transfer. The gold (Au) loaded thionine functionalized GO (graphene oxide) matrix has been shown to immobilize primary antibodies. Thionine works as an electron mediator and interacts with rGO to further increase electrical conductivity. Gold nanoparticles bind with thionine and primary antibodies bound to Au nanoparticles *via* Au–NH_2 bonding. This novel signal amplification strategy demonstrated higher sensitivity toward detection of PSA with a limit of detection of 16.6 fg mL^{-1} and a linear range of 50 fg mL^{-1} to 40 fg mL^{-1}.[83] Bimetallic label-free immunosensors are also used for early diagnosis of pancreatic cancer by using a carbohydrate antigen 19-9 (CA19-9) marker, which is usually present in minute quantities. A bimetallic matrix of polythionine-Au (AuNPs@ PThi) was prepared using a one-pot reaction for developing materials with higher sensitivity by signal amplification. The AuNPs/AuNPs@PThi/GCE was immobilized on a glassy carbon electrode to enhance the electrical properties of the developed immunosensor. The linear range of the sensor was found to be 6.5 to 520 U mL^{-1} with a detection limit of 0.26 U mL^{-1}.[84] Different bimetallic nanocomposite-based electrochemical immunosensors are listed in Table 2.

3.1.3. Trimetallic nanoparticles for signal amplification. Recently, trimetallic materials have also been developed to enhance the electro-catalytic properties useful in signal amplification. Mao *et al.* reported a signal amplification strategy based on the trimetallic nanocomposite of RuPdPt nanoalloy particles for detection of monocyte chemoattractant protein-1 (MCP-1). The primary antibody was immobilized on a rGO-TEPA-Thi-Au (reduced graphene oxide, tetraethylenepentamine, thionine, gold particles) based nanocomposite. r-GO-TEPA provides a larger surface area and more amino groups, which can be

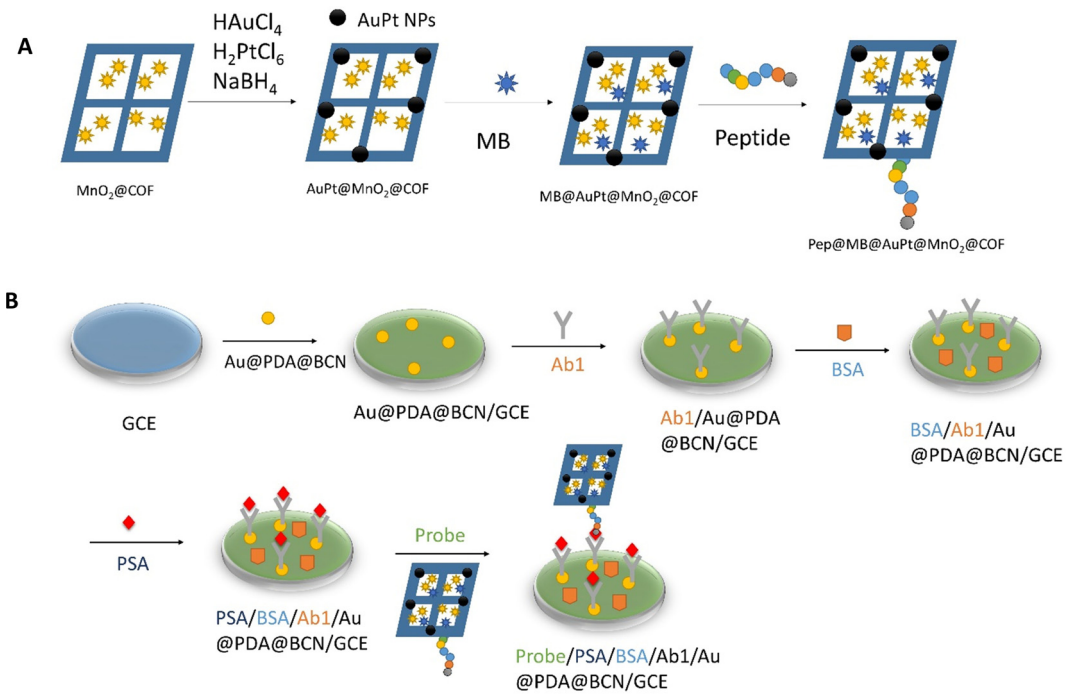

Fig. 5 (A) Preparation of Pep/MB/AuPt@MnO_2@COF bioconjugates. (B) Assembly of the biosensor for the PSA. Redrawn with modification from Zheng *et al.*[81]

Table 2 The bimetallic nanocomposites used in the detection of various biomarkers

Description	Nanocomposite	Linear range	Limit of detection	Ref.
Determination of hydrazine	Nanoparticles of the Au–Cu bimetallic alloy supported on the nano P zeolite carbon paste electrode	0.01–150 mM	0.04 μM	85
Detection of H_2O_2	Pt/Au bimetallic nanoparticles layered on APTMS	5.0 μM to 72000 μM	2.6 μM	86
Nuclear matrix protein 22 (NMP22) detection	NH_2 graphene and Au@Pd/Ag yolk-bimetallic NPs	0.01 to 18 ng mL^{-1}	3.3 pg mL^{-1}	87
Detection of early tumor marker lymphocyte activation gene-3 (LAG-3) protein	The matrix used is of rGO-SnO_2/hollow nano box-MOFs/AuPt alloys (rGO-SnO_2/HNMs/AuPt)	0.01 ng mL^{-1} to 1 μg mL^{-1}	1.1 pg mL^{-1}	86
Early detection of carcinoembryonic antigen (CEA)	Au@Pt alloy with Cu-doped N-doped graphene (Au@Pt DNs/NG/Cu^{2+})	0.5 pg mL^{-1} to 50 ng mL^{-1}	0.167 pg mL^{-1}	88
Detection of H_2O_2 in cancer samples	AuPd alloy and graphene decorated quantum dots	1.0 μM to 18.44 mM	500 nM	89
Detection of PSA	Carbon nanotube dotted with ZnO quantum dots on a Pt/Au alloy	0.001 to 500 ng mL^{-1}	0.61 pg mL^{-1}	90
Detection of cholesterol	AuPt alloy nanoparticles on ionic liquid-chitosan (AuPt–Ch–IL/GCE)	0.05 to 11.2 mM	10 μM	91
Detection of adenosine triphosphate (ATP)	NiFe bimetallic oxide embedded on a mesoporous carbon	5 fg mL^{-1} to 5 ng mL^{-1}	0.98 fg mL^{-1}	92

easily targeted with biological materials or metal nanoparticles. Thionine has electroactive redox properties and is adsorbed on the r-GO-TEPA matrix. Negatively charged gold nanoparticles (Au) were adsorbed onto the positively charged thionine molecules and formed a complete nanocomposite of rGO-TEPA-Thi-Au. Further, higher signal amplification was obtained by using a trimetallic nanocomposite of RuPdPt nanoalloy particles. The developed sensor exhibited ultrasensitive detection of MCP-1 in the range of 20 fg mL^{-1} to 1000 pg mL^{-1}, with a detection limit of 8.9 fg mL^{-1}.[93] Electrochemical sensors have also shown their potential in the detection of cancer cells. A paper-based electrochemical device was also developed that can detect cancer cells using trimetallic dendritic Au@PtPd nanoparticles as a label (Fig. 6). This label was linked with folic acid *via* click chemistry. A separate cellulose paper was modified with Au and folic acid which was used for capturing K-562 cells. To increase the sensitivity, folic acid was attached to capture a higher number of K-562 cells. The linear range was obtained in the range of 1.0×10^2 to

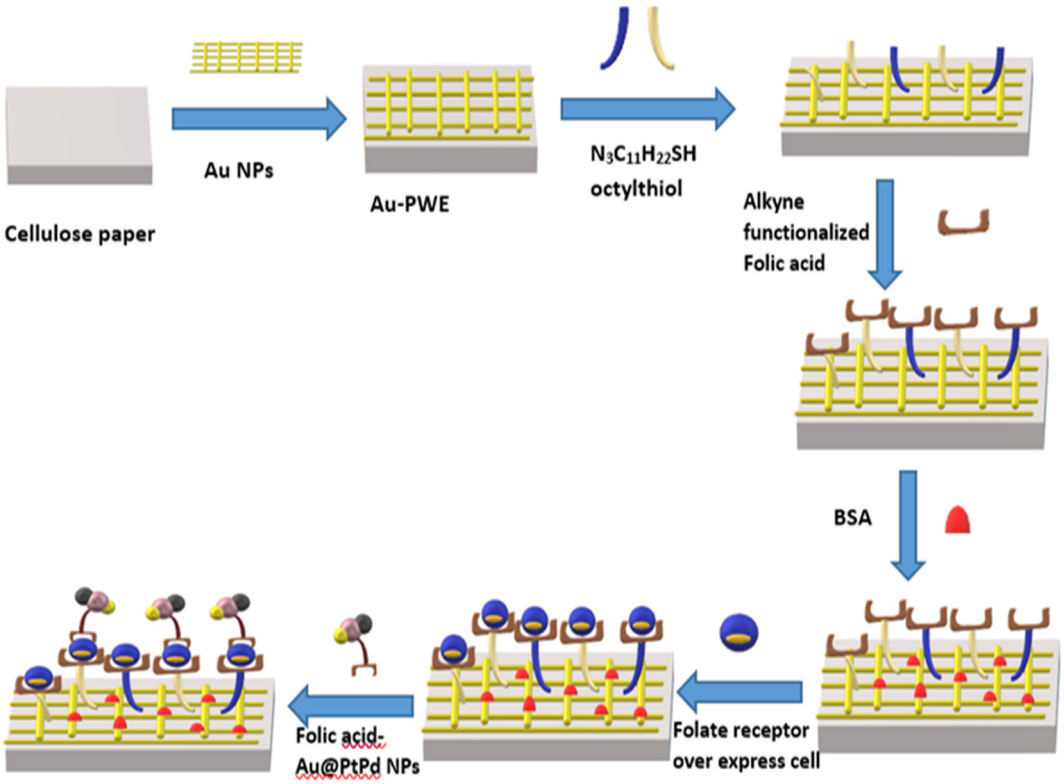

Fig. 6 Schematic representation of the cellulose paper-based electrochemical sensor for detection of cancer cells *via* alkyne functionalized folic acid. Redrawn with modification from Ge *et al.* (2015).[94]

2.0×10^7 cells per mL and the detection limit was 31 cells per mL.[94] Barman *et al.* have electrodeposited trimetallic AuPdPt nanoparticles on the –COOH terminated graphene. Anti-PSA and anti-CEA antibody was then linked by EDC-NHS chemistry on different templates. The electrochemical characterization was done *via* cyclic voltammetry (CV) and differential pulse voltammetry (DPV). For CEA, the antigen linear range was found to be 12 pg mL^{-1} to 85 ng mL^{-1} and the limit of detection was 8 pg mL^{-1}. However, PSA demonstrated a linear range of 3 pg mL^{-1} to 60 ng mL^{-1} and the limit of detection was 2 pg mL^{-1}.[95] An ultrasensitive electrochemical immunosensor was also developed for the detection of prostate-specific antigen (PSA). The label was mesoporous PdPtCu (m-PdPtCu), and the support material was an Au nanoparticle modified glassy carbon electrode with primary anti-PSA. Electrochemical characterization of the developed sensor was done by CV, DPV, and electrochemical impedance spectroscopy (EIS). The linear range was found to be 10 fg mL^{-1} to 100 ng mL^{-1} and the detection limit was 3.3 fg mL^{-1}.[96] In another study, a label-free electrochemical sensor was developed for the early detection of prostate cancer by using a trimetallic material. Trimetallic hollow dendritic AuPtAg nanocrystals were synthesized from L-proline in one pot. The hollow dendritic trimetallic nanocrystals provide a high surface area for binding antibodies and contribute to higher sensitivity. Under optimal conditions, the linear range (0.05–50 ng mL^{-1}) was calculated and the limit of detection (0.017 ng mL^{-1}) was obtained.[97] Different trimetallic nanocomposite-based electrochemical immunosensors are listed in Table 3.

3.2. Polymeric nanocomposites for signal amplification

The conducting polymeric matrix has fascinating electrical conductivity, which contributes to the signal amplification of the sensor to attain higher sensitivity. Electrical conductivity, which may be altered by doping and dedoping, low ionization potential, large electron affinity, and optical characteristics are all inherent qualities of conducting polymers (CPs). Any modification in backbone conjugation and conformation caused by a biological interaction has a major influence on the electrical properties of conducting polymers. The grafting of bioreceptors onto CPs helps in the recognition of biological target with higher sensitivity due to enhanced electrical signals. Polypyrrole (Ppy) has been widely investigated as a CP for sensing applications because of its biocompatibility, strong hydrophilic properties, and high water stability. Zhang *et al.* incorporated ferrocene into the polymer, which led to an increase in the electron transfer rate, causing better conductivity. An aldehyde group was also generated, which was utilized for direct conjugation of antibodies *via* an amine and aldehyde group conjugation strategy. The developed immunosensor demonstrated detection of IgG with a linear range of 0.1 to 20 ng mL^{-1} and the limit of detection was 0.07 ng mL^{-1}.[107]

A microfluidics-based electrochemical immunosensor was developed for the early detection of aspergillosis. The copper nanoparticles coated on a polyvinylpyrrolidone matrix (CuNPs-PVP) were developed to increase the catalytic activity and conductivity of the transducer (Fig. 7). The linear range and limit of detection were found to be 0–2.5 ng mL^{-1} and 0.23 ng mL^{-1} respectively.[108] In another example, quantitative detection of IL-8, which is manifested as a sign of various cancers, was done by fabricating a highly selective immunosensor. The conductive slurry of carbon black super P and polyvinylidene fluoride (PVDF) was utilized to enhance conductivity, along with star-shaped poly glycidyl methacrylate (SPGMA) which was used to immobilize anti-IL-8 on the epoxy group of the polymer. The developed composite was coated on a disposable ITO electrode and was found to be highly sensitive for the detection of IL-8. The limit of detection was found to be 3.3 fg mL^{-1} with a wider linear range of 0.01–3 pg mL^{-1}.[109] Different polymeric nanocomposite-based electrochemical immunosensors used for the detection of various biomarkers are listed in Table 4.

3.2.1. Molecularly imprinted polymer-based electrochemical immunosensors. Molecularly imprinted polymers (MIPs) are developed using a template polymerization process of creating

Table 3 Trimetallic nanocomposites used in the detection of various biomarkers

Description	Nanocomposite	Linear range	Limit of detection (LOD)	Ref.
Detection of H_2O_2 and prostate-specific antigen (PSA)	COOH-AgPtPd/NH_2-rGO nanocomposite	The linear range of prostate-specific antigen was 4 fg mL^{-1} to 300 ng mL^{-1}	LOD of H_2O_2 and prostate-specific antigen was 0.2 nM and 4 fg mL^{-1} respectively	99
Detection of semaphorin3E (Sema 3E)	The trimetallic nanocomposite of CuAuPd nanowire networks	100 fg mL^{-1} to 10 ng mL^{-1}	LOD of 1.5 fg mL^{-1} (S/N = 3)	100
Detection of glucose	Trimetallic PtAuPd nanocomposite	0.005 to 9 mM	LOD of 0.13 μM (S/N = 3)	101
Detection of ascorbic acid (AA), dopamine (DA), acetaminophen (AP) and tryptophan (TP)	The trimetallic nanocomposite of (Au/Ag/Pd) NPs/EPGr	Linear range of AA, DA, AP and TP was 5–650 μM, 1–700 μM, 5–700 μM and 1–600 μM respectively	LOD of AA, DA, AP and TP was 0.24 ± 0.03, 0.02 ± 0.01, 0.12 ± 0.04 and 0.03 ± 0.01 μM, respectively	102
Detection of serum human epididymis protein 4 (HE4)	Trimetallic AgPtCo nanodendrites (NDs) along with magnetic nanocomposites (Fe_3O_4@SiO_2@Au MNCs)	The linear range was 0.001–50 ng mL^{-1}	LOD of 0.487 pg mL^{-1}	103
Dynamic monitoring of hydrogen peroxide production by cancerous cells	Trimetallic AuPtAg nanoalloy with poly(diallyl dimethylammonium chloride)-capped reduced graphene oxide	Linear range from 0.05 μM to 5.5 mM	LOD of 1.2 nM	104
Detection of cardiac troponin I	Trimetallic alloyed AuPtPd porous fluffy-like nanodendrites (AuPtPd FNDs)	Linear range of 0.01–100.0 ng mL^{-1}	LOD of 3 pg mL^{-1}	105
Detection of breast cancer	Trimetallic AuPtPd nanocomposites along with reduced graphene oxide	Linear range from 0.005 μM to 6.5 mM	LOD of 2 nM	106

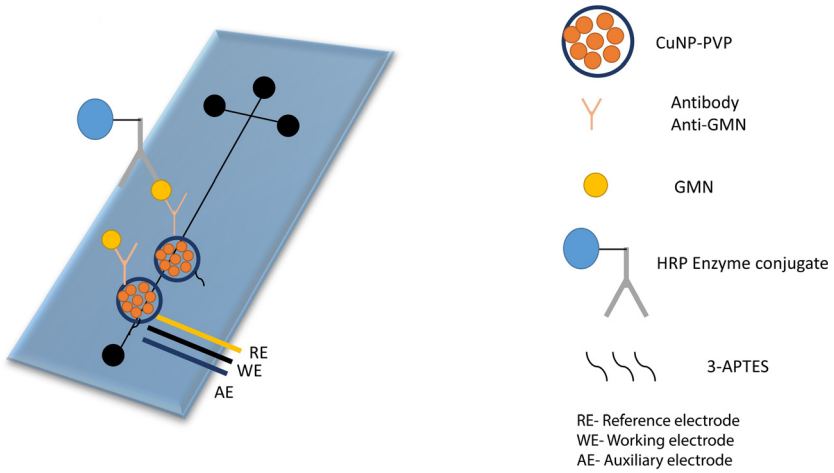

Fig. 7 Representation of the glass microfluidic surface modification and the immunological reaction. Anti-GMN monoclonal antibodies were covalently bound to CuNPs-PVP. Redrawn with modification from S. V. Piguillem *et al.*[108]

artificial recognition sites in a macromolecular matrix that is similar to the target molecule.[117] The molecular imprinted polymer-based electrochemical biosensor has gained attention in the field of diagnostics. The imprinted polymer was exposed as an artificial enzyme site or antibody-mimicking polymer substance. The size and form of cavities are important criteria in distinguishing MIPs from biomarkers. The chemical identification of biomarkers is also a critical parameter. Non-covalent, semi-covalent, and covalent chemical recognition techniques are the types of MIPs. Non-covalent recognition, which comprises hydrogen bonds, hydrophobic contacts, and electrostatic interactions, is the most extensively used for the construction of MIPs/SIPs due to its versatility. Recently, Pereira and colleagues fabricated a molecular imprinted electrochemical immunosensor where poly(toluidine blue) was used as a molecular imprinting polymer against the CA 15-3 marker for the diagnosis of breast cancer (Fig. 8). The toluidine blue monomer was immobilized on a gold electrode *via* conjugation between aldehyde functional groups and an aromatic amine group of phenothiazine. The toluidine blue modified electrode was electropolymerized in the presence of CA 15-3. The linearity of the sensor was found to be 0.10 U mL^{-1} to 100 U mL^{-1} and the limit of detection was below 0.10 U mL^{-1}.[98] Usually, more than one marker is desirable for the early diagnosis of cancer. It was also demonstrated that an electrochemical immunosensor based on molecularly imprinted polymers can simultaneously detect EGFR and VEGF. For better sensitivity in a sensor, antibody conjugated nano-liposomes having Cd(II) and Cu(II) cations were used. The antibody conjugated liposome forms a complex with EGFR and VEGF. The lysis buffer was then added to deform the Ab_{EGFR}@Cd^{+2}LPs and Ab_{VEGF}@Cu^{+2}LPs complexes, and the released Cu^{+2} and Cd^{+2} were quantified *via* potentiometric stripping. The linearity of the

Table 4 Polymeric nanocomposites used in the detection of various markers

Description	Nanocomposite	Linear range	Limit of detection (LOD)	Technology	Matrix	Ref.
Detection of didanosine (DDI)	Pencil graphite electrode (PGE) modified with a polymer such as polypyrrole (PPy) and reduced graphene oxide (rGO) (PGE/PPy/rGO)	0.02–50.0 μM	8.0 nM	EIS	Pharmaceutical samples	110
Detection of tramadol	PGE/CuO-NPs/PPy	5.0 nM–380 μM	1.0 nM	Square wave voltammetric method	Drug sample	111
Detection of glucose	GOx immobilized on nanoPANi (polyaniline nanotubes)	0.01–5.5 mM	0.3 ± 0.1 μM	Cyclic voltammogram	Real clinical samples	112
Detection of organophosphates	PAn-PPy-MWCNTs copolymer	0.01 to 0.5 μg mL^{-1} and from 1 to 25 μg mL^{-1}	1.0 ng mL^{-1}	EIS and cyclic voltammetry		113
Simultaneous detection of Pb^{2+} and Cu^{2+}	Au@PANI nanocomposite	Pb^{2+} linear range is 0.02–0.72 μM Cu^{2+} linear range is 0.08–2.4 μM	Pb^{2+} with an LOD of 0.003 Cu^{2+} LOD is 0.008 μM	Square wave anodic stripping voltammetry (SWASV)	—	114
Detection of prostate specific antigen (PSA)	Nanocomposite of AuNPs/nano-PEDOT-graphene aerogel	0.0001–50 ng mL^{-1}	0.03 pg mL^{-1}	Differential pulse voltammetry (DPV)	PSA in real samples	115
Detection of an anti-diabetic drug (Metformin)	GNF-PMB/modified SnO_2/F glass	10–103 μM	0.1 nM	CV and EIS	Urine, serum	116

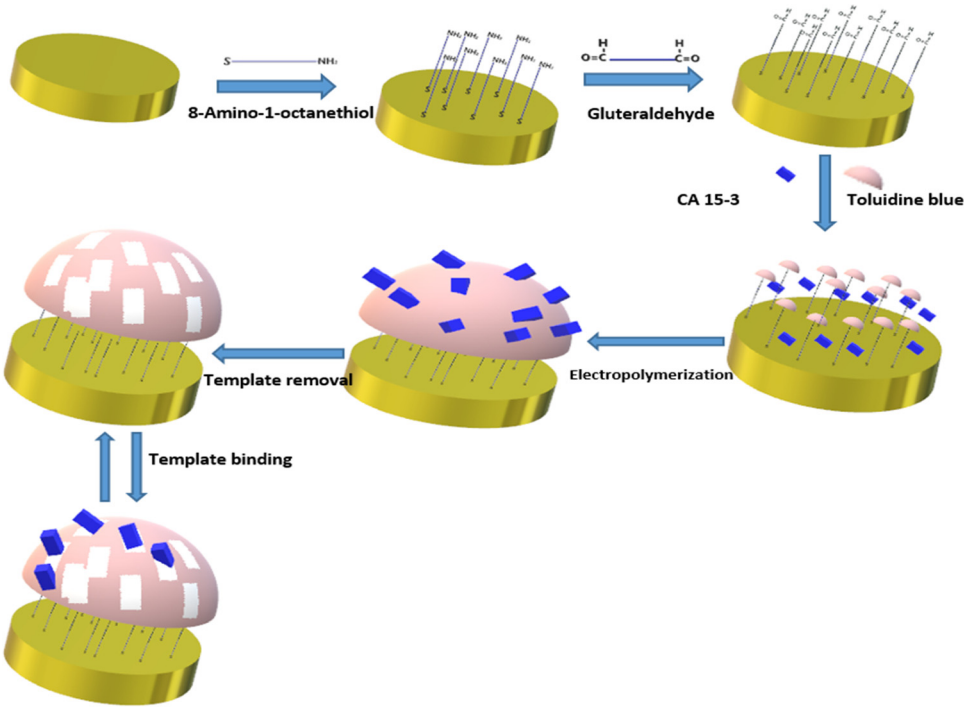

Fig. 8 Schematic representation of imprinted polymer toluidine blue for diagnosis of breast cancer antigen CA 15-3. Redrawn with modification from Ribeiro *et al.* (2018).[98]

sensor for EGFR and VEGF was found to be 0.05–5000 pg mL^{-1} and 0.01–7000 pg mL^{-1}, respectively. The limit of detection was 0.01 pg mL^{-1} and 0.005 pg mL^{-1} for EGFR and VEGF, respectively.[118]

3.3. Semiconducting material based electrochemical immunosensor

A semiconductor as a substrate can also be used as a monocomponent and multi-component. Interestingly, a biosensor was developed for the diagnosis of bladder cancer by coating Bi_2S_3 nanocrystals on the electrode followed by immobilization of antibodies. The detection of CK18 was in the range of 1–1000 pg mL^{-1} and LOD was found to be 1.87 fM (fmol L^{-1}).[119] The semiconductor can be coupled with a composite, metal, tandem structure, heterostructure, *etc.* Additionally, these materials have been doped with metal ions or linked with metal nanoparticles to improve their electrical conductivity. Widely used metal oxide semiconductors are available in a variety of shapes and sizes, including rods, stars, flowers, cones, porous or thick films, and so on. Graphene-based composites demonstrated application in developing electrodes with higher sensitivity during the last decade, but graphene has a significant limitation in possessing a smaller bandgap.[120] To overcome this limitation, quantum dots and carbon dot-based nanocomposites have been developed for better electron transfer.[121] Recently, Srivastava *et al.* have compared two approaches for signal amplification based on an aptasensor and immunosensor modified on a graphene quantum dots-gold nanorods (GQDs-AuNRs) composite coated on glassy carbon for the detection of the PSA antigen for diagnosing prostate cancer. It was found that GQDs-AuNRs act as excellent electron acceptor-transporters. The limit of detection for both sensors was found to be the same under the optimal condition (0.14 ng mL^{-1}).[106] An electrochemical immunosensor was also developed for fast TB diagnosis using nanotriplex comprising graphene quantum dots (GQDs), Ag NPs, and Fe_3O_4 as a nanocomposite material (Fig. 9). It has had a huge impact on sensor development by providing high sensitivity and selectivity, compared to other conventional techniques. The developed nanotriplex has several advantages, including higher surface area, high adsorption ability, and the inherent property of a nanocatalyst that reduces H_2O_2 and improves mass transport. Ag NPs improved the conductivity and prevented the agglomeration of Fe_3O_4. GQDs also provide a higher coverage area for the immobilization of an antibody and demonstrate catalytic activity towards H_2O_2. Thus, Fe_3O_4/GQDs act in a synergistic way for signal amplification. The fabricated sensor showed a linear response in the range of 0.005 to 500 μg mL^{-1}, which was characterised by differential pulse voltammetry (DPV), demonstrating a good linear correlation coefficient of 0.997 (Fig. 10a). It indicates good selectivity of the developed immunosensor for the target analyte (CFP-10) against other similar-sized proteins (Fig. 10b). The limit of detection of the developed sensor was found to be 0.33 ng mL^{-1}.[122] Researchers used a combination of two different semiconductors to increase the sensitivity of the biosensor and also incorporated semiconductors into the polymeric matrices to enhance the performance of the biosensor. Researchers fabricated biosensors for the detection of dengue where graphene oxide was incorporated into the polymeric matrix composite (PMCs), which included *N*-vinylpyrrolidone acrylamide, methyl methacrylate, and methacrylic 144 acids. This sensor

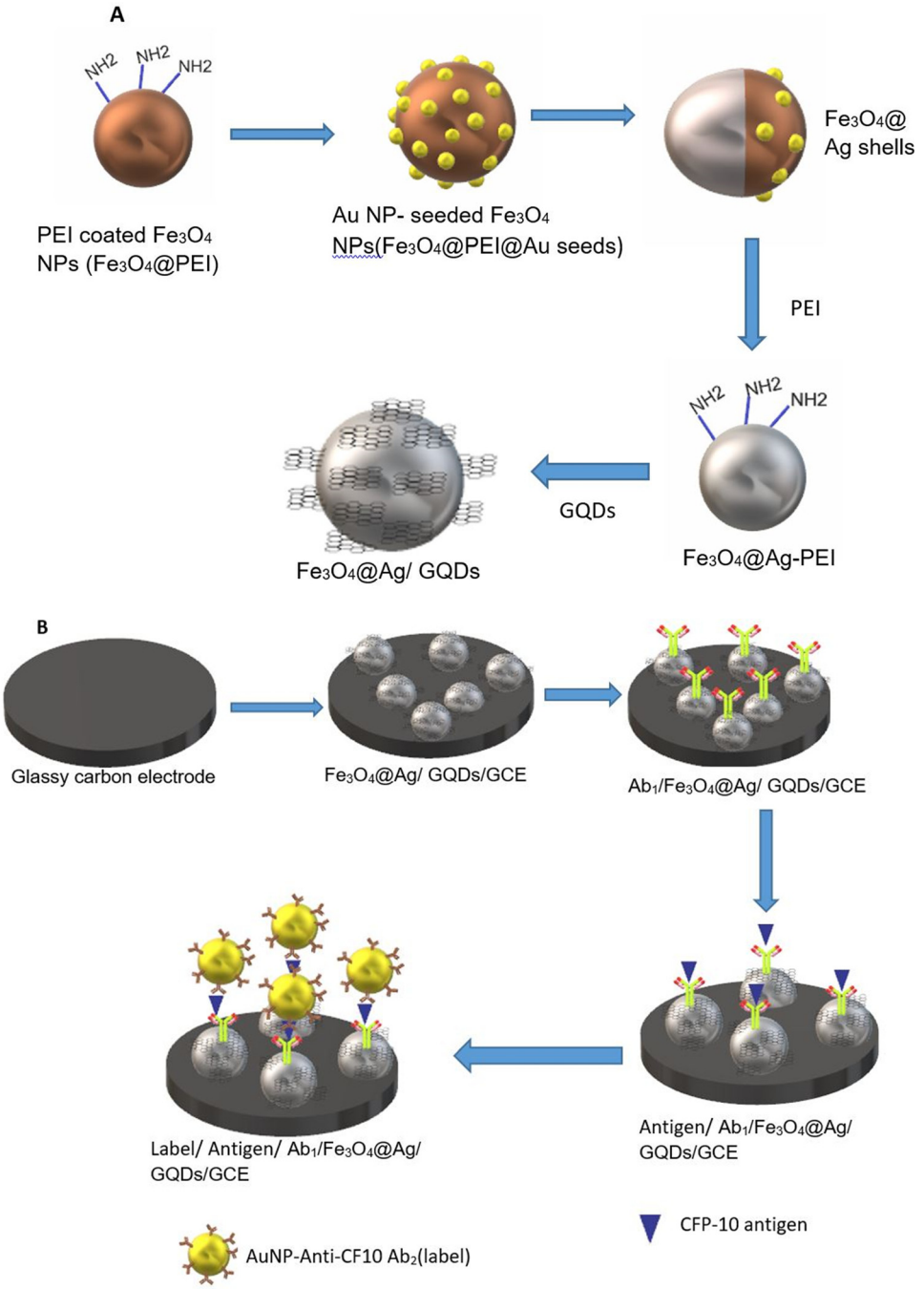

Fig. 9 (A) Schematic representation of nanocomposite preparation. (B) Fabrication of the glassy carbon electrode. Redrawn with modification from Tufa *et al.* (2018).[122]

provided higher sensitivity, attributable to permitting the accommodation of small molecules. The LOD of the developed sensor was 0.12 pfu mL^{-1}.[123] In another example, researchers developed a sensor by modifying the carbon electrode using lead sulfide (PbS) colloidal quantum dots for the diagnosis of allergic rhinitis by detecting the biomarker eosinophil cationic protein *via* DPV. The limit of detection was found to be 0.508 pg mL^{-1} with a response time of about 30 seconds.[124]

The incorporation of inorganic, organic, and semiconductor elements into a gold nanoparticle could provide oriented immobilization. Sheng Feng Huang *et al.* fabricated a sensor by modifying the surface of the working electrode with a coating of gold and molybdenum disulfide (semiconductor) leading to the oriented immobilization of antibodies *via* bonding with multifunctional DNA constructed onto the modified electrode. The oriented immobilization is attributed to the spatially confined assembly (SCA) strategy mediated by DNA and the MoS_2/gold NPs favour the spatial attachment of thiol peptides and reduce the spatial repulsion between the antibody molecules. Hence, a sensitive and accurate sensor is achieved for the

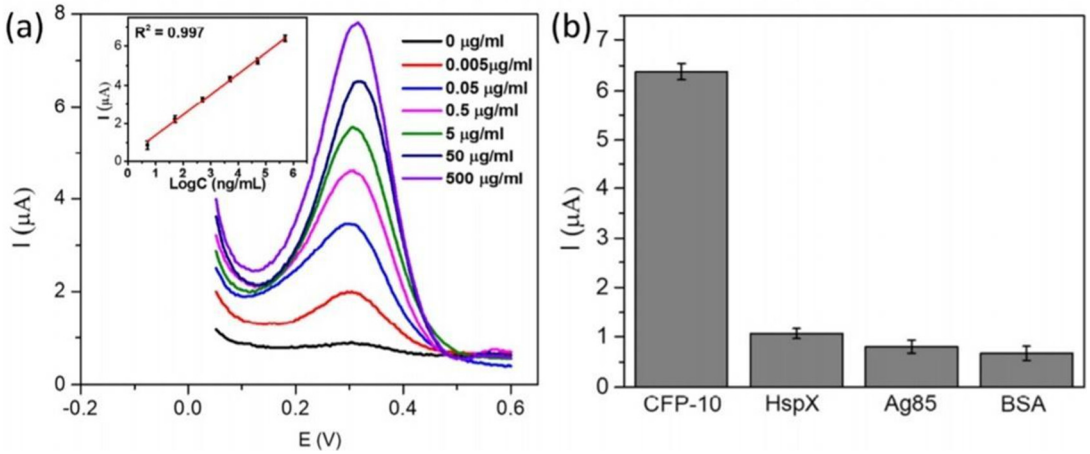

Fig. 10 (a) DPV at different concentrations for the detection of CFP-10. (b) Differential pulse voltammetry responses of immune sensors to 0.5 mg mL^{-1} CFP-10, 1.8 mg mL^{-1} HspX protein of Mtb (16 kDa), 3.57 mg mL^{-1} Ag85, and 2% BSA. Reproduced from Tufa *et al.* (2018).[122]

detection of rituximab with an LOD of 56.4 fM and an RSD of less than 6.5%.[125]

3.4. Carbon materials and novel 2D materials for signal amplification

Carbon-based materials used for signal amplification in electrochemical biosensing were demonstrated to be excellent electrode materials for signal transmission as separators, collectors, catalysts, and with resistance towards electrode fouling due to lower overpotential electron transfer and in the regulation of the electron transfer process.[126] The carbon-based materials are ideal electrode materials for application in biosensors due to their higher stability and shelf life. The carbon-based materials usually increase the electron transfer rate of the material. Carbon nanomaterials in a wide range of allotropes, such as single or multi-wall carbon nanotubes (SWCNT/MWCNT), carbon nanodots, carbon nanohorns (CNH), carbon nanofibers (CNF), graphene derivatives, carbon nanoparticles, and nitrogen-doped carbon materials, have all been widely used as electrode materials for various sensing applications, depending on the demand. The carbon nanotubes were also incorporated in MOF-808 (metal–organic framework) to increase its conductivity. The developed sensor provides a high surface area and good electrochemical properties with a linear range of 0.001–0.1 and 0.1–30 ng mL^{-1}, and the limit of detection is 0.5 pg·mL^{-1}.[127] Gulati *et al.* have developed an electrochemical immunosensor for the early detection of leukemia using a single-wall carbon nanotube (SWCNT). The SiO_2/Si electrode was modified with the SWCNT for signal amplification and better sensitivity.[128] The electrode was functionalized with 1% 3-glycidoxy-propyl-trimethoxy silane (3-GPMS), which contains highly reactive epoxy groups which react with the amino groups of antibodies to form cyanide covalent bonding. It has demonstrated higher immobilization of anti-*P*-glycoprotein antibodies on SWCNTs, which contributes to higher sensitivity. The linearity range was found to be 1.5×10^3 to 1.5×10^7 cells per mL and the limit of detection was 19 cells per mL.[129] The electrochemical sensor faces a major challenge in the residence time of the analyte. Wang *et al.* have developed a paper-based integrated microfluidic channel to overcome the limitation associated with the residence time of the analyte (Fig. 11).[131] The developed sensor was used for the detection of 17β-estradiol. The nanocomposite of multiwall carbon nanotubes (MWCNT)/thionine (THI)/AuNPs was created, in which the MWCNT has a larger surface area and faster electron transfers, while THI acts as an electrochemical mediator and covalently binds with MWCNT *via* stacking. AuNPs not only provide better conductivity but also facilitate better interaction with antibodies.[130] The performance of the modified immunosensor was characterized *via* differential pulse voltammetry (DPV) (Fig. 12A). The peak current is decreased as the concentration of the analyte is increased, representing a decrease in conductivity, which shows a good linear range of 10 pg mL^{-1} to 100 ng mL^{-1} and the limit of detection (LOD) was found to be 10 pg mL^{-1} (Fig. 12B).[131]

The modification of the transducer with different 2D materials rather than graphene was also reported, such as transition metal dichalcogenides (TMDs), boron nitride (BN), and graphite-carbon nitride (g-C_3N_4).[132] The sensing performance of these new 2D materials was tested and compared with that of the 2D molybdenum disulfide (MoS_2) layered nanosheet and core–shell structured Au@SiO_2@Au modified electrochemical aptasensor. The developed electrochemical aptasensor was used for determining cardiac troponin-I. The study demonstrated that a sensor modified with an aptamer-MoS_2 nanosheet has higher sensitivity than an aptamer-Au@SiO_2@Au core–shell modified sensor. Higher sensitivity could be attributed to the properties of 2D molybdenum disulfide (MoS_2) such as semiconductivity, indirect-to-direct bandgap transition (from 1.2 to 1.9 eV), and layer structured nanosheets. From the comparison study, the limit of detection for the aptamer-MoS_2 nanosheet was found to be 0.95 pM and for aptamer-Au@SiO_2@Au, the limit of detection was 1.23 pM.[133] Su *et al.* fabricated an electrochemical immunosensor for the detection of carcinoembryonic antigen using a modified glassy carbon electrode with the MoS_2-Prussian blue nanocubes (PBNCs) nanohybrid 2D nanocomposite. The limit of detection was 0.54 pg mL^{-1} and the linear range was found to be 0.005–10 ng mL^{-1}. The extraordinary electrocatalytic activity of Prussian

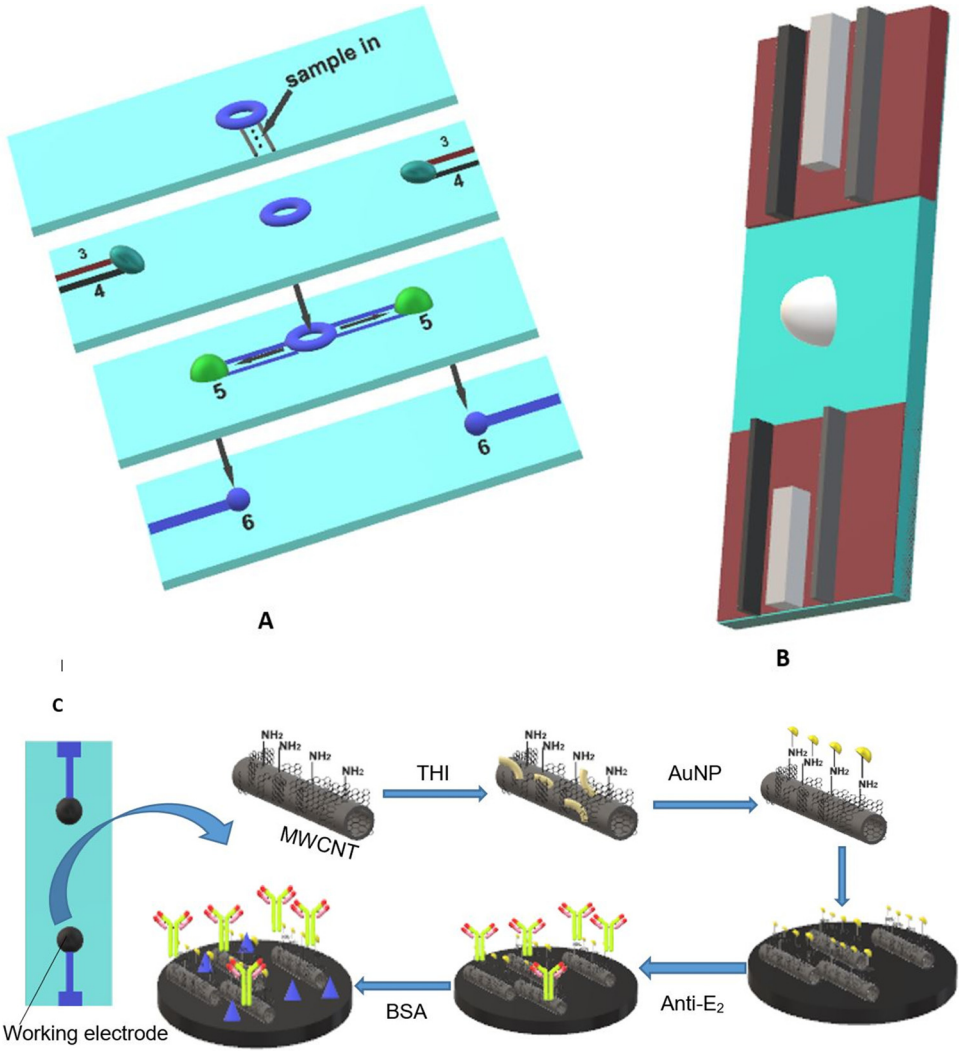

Fig. 11 (A) Schematic representation of the paper-based microfluidic system where (3) counter electrode, (4) reference electrode, (5) site for reaction, and (6) working electrode. (B) Paper-based integrated sensor chip. (C) Fabrication of a glassy carbon electrode with a nanocomposite (MWCNT/THI/AuNPs). Redrawn with modification from Wang *et al.* (2018).[131]

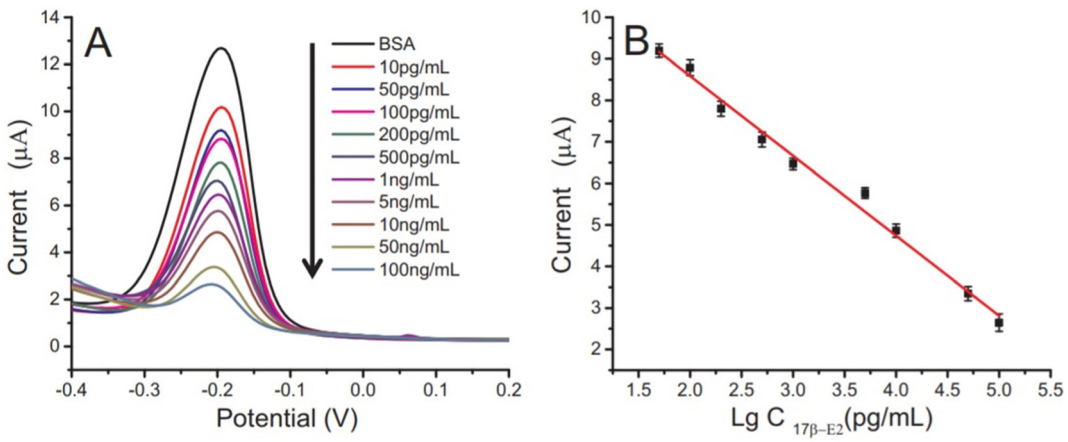

Fig. 12 (A) Differential pulse voltammetry of different concentrations of 17β-E2. (B) Microfluidic paper-based immunodevice calibration curve towards 17β-E2. Reproduced from Wang *et al.* (2018).[131]

blue and the higher surface area and conductivity of MoS_2 could be one of the key explanations behind the higher sensitivity. In an actual sample, the developed sensor has further shown improvement in the sensitivity and selectivity for CEA.[134] A label-free electrochemical immunosensor for insulin determination was done using a novel nanocomposite of Pd NPs@3D MoS_x material. Pd NPs incorporated into 3D MoS_2 provide sufficient surface area for antibody attachment *via* Pd–N bonding, as well as exhibit catalytic activity towards H_2O_2. They discovered a linear association between log insulin concentrations of 0.01 to 100 ng mL^{-1} and an LOD of 3.0 pg mL^{-1} (S/N = 3).

4. Conclusion

The techniques of immobilisation and strategies to design the platform appropriate for immobilisation have become one of the trendiest fields of research due to the necessity for ultrasensitive, quick, and early disease diagnostics. The creation of ultrasensitive biosensors still faces various challenges. The ultimate objective of this discipline is the use of various strategies that not only boost the biosensing capabilities compared to conventional platforms but also meet the demand in life sciences and clinical diagnostics. This is possible using appropriate immobilisation techniques, including non-covalent, covalent, and site-directed immobilisation. Several nanotechnology-based nanomaterials have shown an innovative way of modification as a substrate for high-sensitive analysis. We have discussed the importance of different immobilization techniques and their effects on the analysis of electrochemical signals. We introduced different types of functional nanomaterials (MWCNTs, graphene, metallic nanoparticles, polymeric materials, gold nanoparticles, nanowire, and molecule imprinted polymers), which are generally utilized for modification of electrodes as supporting matrices due to their high electrical conductivity, huge surface area, *etc.* These surfaces are functionalized with various groups (silane, thiols, and aldehydes) for effective immobilization. We also talked about how to improve the sensitivity and linearity of the electrochemical sensor by using a site-oriented conjugation strategy and labelling techniques. These strategies can be utilized for the point-of-care version of the electrochemical sensor platform. Additionally, a number of techniques for fabricating substrate platforms have been developed, including the utilisation of nanomaterials, metal semiconductors, and polymers for signal amplification and diagnostic repeatability. Excellent electronic, optical, and photoelectrochemical signal transduction abilities are among the characteristics of these nanomaterials and other materials acting as transducers, and they can be used to create a new generation of biosensing devices and to detect a particular antibody in a particular disease. Overall, a superior combination of materials science and electrochemistry principles is the main player in the development of a reliable, sensitive electrochemical sensor for a modern generation.

Author's contribution

M. P. and A. S. conceived the idea, M. P. and M. A. wrote the draft, and A. S. edited the manuscript.

Conflicts of interest

The authors do not have any competing interests.

Acknowledgements

This work is financially supported by the Department of Pharmaceuticals, Ministry of Chemicals and Fertilizers, Government of India.

References

1 M. Choudhary and K. Arora, *Biosensor Based Advanced Cancer Diagnostics*, Elsevier, 2022, pp. 123–151.
2 M. B. Akolpoglu, U. Bozuyuk, P. Erkoc and S. Kizilel, *Advanced Biosensors for Health Care Applications*, Elsevier, 2019, pp. 249–262.
3 D. Antuña Jiménez, G. Díaz Díaz, M. D. C. Blanco López, M. J. Lobo Castañón, A. J. Miranda Ordieres and P. Tuñón Blanco, *Molecularly Imprinted Sensors*, 2012.
4 L. Wang, *Sensors*, 2017, **17**, 2420.
5 U. Z. Mohd Azmi, N. A. Yusof, N. Kusnin, J. Abdullah, S. Suraiya, P. S. Ong, N. H. Ahmad Raston, S. F. Abd Rahman and M. F. Mohamad Fathil, *Sensors*, 2018, **18**, 3926.
6 P. Habeen, L. Ji-Young, K. Dong-Chul, K. Younggook and C. Junhoe, International Conference on Nano-Bio Sensing, Imaging, and Spectroscopy 2017, *Proc. SPIE*, 2017, **10324**, 1032405.
7 R. Singh, S. Hong and J. Jang, *Sci. Rep.*, 2017, **7**, 1–11.
8 L. Ruiyi, C. Fangchao, Z. Haiyan, S. Xiulan and L. Zaijun, *Biosens. Bioelectron.*, 2018, **119**, 156–162.
9 L. V. Tarditto, M. A. Zon, H. G. Ovando, N. R. Vettorazzi, F. J. Arévalo and H. Fernández, *Talanta*, 2017, **174**, 507–513.
10 M. Li, Y. Zheng, W. Liang, Y. Yuan, Y. Chai and R. Yuan, *Chem. Commun.*, 2016, **52**, 8138–8141.
11 G. Rocchitta, A. Spanu, S. Babudieri, G. Latte, G. Madeddu, G. Galleri, S. Nuvoli, P. Bagella, M. I. Demartis and V. Fiore, *Sensors*, 2016, **16**, 780.
12 S. K. Thomas, W. D. Jamieson, R. E. Gwyther, B. J. Bowen, A. Beachey, H. L. Worthy, J. E. Macdonald, M. Elliott, O. K. Castell and D. D. Jones, *Bioconjugate Chem.*, 2019, **31**, 584–594.
13 R. B. D. Cruz, G. A. Alonso, R. Muñoz and J.-L. Marty, *Biosensors: Recent Advances and Mathematical Challenges*, 2014, pp. 143–161.
14 M. K. Masud, J. Na, M. Younus, M. S. A. Hossain, Y. Bando, M. J. Shiddiky and Y. Yamauchi, *Chem. Soc. Rev.*, 2019, **48**, 5717–5751.
15 J. Lei and H. Ju, *Chem. Soc. Rev.*, 2012, **41**, 2122–2134.

16 M. Islam, M. Iqbal, T. Rahman and A. Y. M. Abdullah, BS thesis, Brac University, 2019.
17 S. Gao, J. M. Guisán and J. Rocha-Martin, *Anal. Chim. Acta*, 2022, **1189**, 338907.
18 J. Hu, Y. Yu, J. C. Brooks, L. A. Godwin, S. Somasundaram, F. Torabinejad, J. Kim, C. Shannon and C. J. Easley, *J. Am. Chem. Soc.*, 2014, **136**, 8467–8474.
19 A. Kausaite-Minkstimiene, A. Ramanaviciene, J. Kirlyte and A. Ramanavicius, *Anal. Chem.*, 2010, **82**, 6401–6408.
20 M. Shen, J. F. Rusling and C. K. Dixit, *Methods*, 2017, **116**, 95–111.
21 G. Ruiz, K. Tripathi, S. Okyem and J. D. Driskell, *Bioconjugate Chem.*, 2019, **30**, 1182–1191.
22 L. Zhang, Y. Mazouzi, M. Salmain, B. Liedberg and S. Boujday, *Biosens. Bioelectron.*, 2020, **165**, 112370.
23 A. Kaushik, A. Yndart, S. Kumar, R. D. Jayant, A. Vashist, A. N. Brown, C.-Z. Li and M. Nair, *Sci. Rep.*, 2018, **8**, 1–5.
24 Z.-P. Chen, Z.-F. Peng, P. Zhang, X.-F. Jin, J.-H. Jiang, X.-B. Zhang, G.-L. Shen and R.-Q. Yu, *Talanta*, 2007, **72**, 1800–1804.
25 S. Goodchild, T. Love, N. Hopkins and C. Mayers, *Adv. Appl. Microbiol.*, 2005, **58**, 185–226.
26 M. Tonigold, J. Simon, D. Estupiñán, M. Kokkinopoulou, J. Reinholz, U. Kintzel, A. Kaltbeitzel, P. Renz, M. P. Domogalla and K. Steinbrink, *Nat. Nanotechnol.*, 2018, **13**, 862–869.
27 Y. Shen, Y. Zhang, M. Liu, X. Liu, H. Guo, X. Zhang, C. Zhang, H. Li and S. Yao, *Talanta*, 2015, **141**, 288–292.
28 M. H. Nawaz, A. Hayat, G. Catanante, U. Latif and J. L. Marty, *Anal. Chim. Acta*, 2018, **1026**, 1–7.
29 R. Raghav and S. Srivastava, *Biosens. Bioelectron.*, 2016, **78**, 396–403.
30 Y. Liu and J. Yu, *Microchim. Acta*, 2016, **183**, 1–19.
31 M. K. Masud, R. G. Mahmudunnabi, N. B. Aziz, C. H. Stevens, D. Do-Ha, S. Yang, I. P. Blair, M. S. A. Hossain, Y. B. Shim and L. Ooi, *ChemElectroChem*, 2020, **7**, 3459–3467.
32 M. N. Islam, M. K. Masud, N.-T. Nguyen, V. Gopalan, H. R. Alamri, Z. A. Alothman, M. S. Al Hossain, Y. Yamauchi, A. K. Lamd and M. J. Shiddiky, *Biosens. Bioelectron.*, 2018, **101**, 275–281.
33 M. A. Wronska, I. B. O'Connor, M. A. Tilbury, A. Srivastava and J. G. Wall, *Adv. Mater.*, 2016, **28**, 5485–5508.
34 S. N. Mthembu, A. Sharma, F. Albericio and B. G. de la Torre, *ChemBioChem*, 2020, **21**, 1947–1954.
35 J.-a A. Ho, W.-L. Hsu, W.-C. Liao, J.-K. Chiu, M.-L. Chen, H.-C. Chang and C.-C. Li, *Biosens. Bioelectron.*, 2010, **26**, 1021–1027.
36 M. Gwiazda, S. K. Bhardwaj, E. Kijeńska-Gawrońska, W. Swieszkowski, U. Sivasankaran and A. Kaushik, *Biosensors*, 2021, **11**, 227.
37 A. A. Karyakin, G. V. Presnova, M. Y. Rubtsova and A. M. Egorov, *Anal. Chem.*, 2000, **72**, 3805–3811.
38 N. J. Alves, N. Mustafaoglu and B. Bilgicer, *Biosens. Bioelectron.*, 2013, **49**, 387–393.
39 N. J. Alves, N. Mustafaoglu and B. Bilgicer, *Bioconjugate Chem.*, 2014, **25**, 1198–1202.
40 M. Iijima, M. Somiya, N. Yoshimoto, T. Niimi and S. I. Kuroda, *Sci. Rep.*, 2012, **2**, 1–5.
41 N. G. Welch, J. A. Scoble, B. W. Muir and P. J. Pigram, *Biointerphases*, 2017, **12**, 02D301.
42 D. Saerens, L. Huang, K. Bonroy and S. Muyldermans, *Sensors*, 2008, **8**, 4669–4686.
43 S. Sharma, H. Byrne and R. J. O'Kennedy, *Essays Biochem.*, 2016, **60**, 9–18.
44 I. Vikholm-Lundin, S. Auer, M. Paakkunainen, J. A. Määttä, T. Munter, J. Leppiniemi, V. P. Hytönen and K. Tappura, *Sens. Actuators, B*, 2012, **171**, 440–448.
45 E. Sánchez-Tirado, A. González-Cortés, P. Yáñez-Sedeño and J. Pingarrón, *Analyst*, 2016, **141**, 5730–5737.
46 Y. Yao, J. Bao, Y. Lu, D. Zhang, S. Luo, X. Cheng, Q. Zhang, S. Li and Q. Liu, *Sens. Actuators, B*, 2016, **222**, 127–132.
47 H. Afsharan, B. Khalilzadeh, H. Tajalli, M. Mollabashi, F. Navaeipour and M.-R. Rashidi, *Electrochim. Acta*, 2016, **188**, 153–164.
48 Y. Luo, A. M. Asiri, X. Zhang, G. Yang, D. Du and Y. Lin, *RSC Adv.*, 2014, **4**, 54066–54071.
49 C. You, R. Dai, X. Cao, Y. Ji, F. Qu, Z. Liu, G. Du, A. M. Asiri, X. Xiong and X. Sun, *Nanotechnology*, 2017, **28**, 365503.
50 R. Elshafey, A. C. Tavares, M. Siaj and M. J. B. Zourob, *Biosens. Bioelectron.*, 2013, **50**, 143–149.
51 C. Zhang, L. Liu, H. Li, J. Hu, J. Zhang, H. Zhou, Z. Zhang and X. Du, *Sens. Actuators, B*, 2022, **353**, 131074.
52 S. Biswas, Q. Lan, Y. Xie, X. Sun and Y. Wang, *ACS Appl. Mater. Interfaces*, 2021, **13**, 3295–3302.
53 M. Khanwalker, R. Fujita, J. Lee, E. Wilson, K. Ito, R. Asano, K. Ikebukuro, J. LaBelle and K. Sode, *Biosens. Bioelectron.*, 2022, **200**, 113901.
54 S. Chebil, I. Hafaiedh, H. Sauriat-Dorizon, N. Jaffrezic-Renault, A. Errachid, Z. Ali and H. Korri-Youssoufi, *Biosens. Bioelectron.*, 2010, **26**, 736–742.
55 J. Zapatero-Rodríguez, S. Liébana, S. Sharma, S. Gilgunn, G. A. Drago and R. O'Kennedy, *Bionanoscience*, 2018, **8**, 680–689.
56 S. Sanli, H. Moulahoum, O. Ugurlu, F. Ghorbanizamani, Z. P. Gumus, S. Evran, H. Coskunol and S. Timur, *Talanta*, 2020, **217**, 121111.
57 W. Lee, B.-K. Oh, W. H. Lee and J.-W. Choi, *Colloids Surf., B*, 2005, **40**, 143–148.
58 X. Liu, Y. Wen, W. Wang, Z. Zhao, Y. Han, K. Tang and D. Wang, *Microchim. Acta*, 2020, **187**, 1–10.
59 S. B. Dulay, R. Gransee, S. Julich and H. Tomaso, *Biosens. Bioelectron.*, 2014, **59**, 342–349.
60 Y. Jung, J. M. Lee, H. Jung and B. H. Chung, *Anal. Chem.*, 2007, **79**, 6534–6541.
61 P. Hashemi, A. Afkhami, B. Baradaran, R. Halabian, T. Madrakian, F. Arduini, T. A. Nguyen and H. Bagheri, *Anal. Chem.*, 2020, **92**, 11405–11412.
62 Y. Zhang and Q. Wei, *J. Electroanal. Chem.*, 2016, **781**, 401–409.
63 S. A. Lim and M. U. Ahmed, *RSC Adv.*, 2016, **6**, 24995–25014.
64 D. Lin, R. G. Pillai, W. E. Lee and A. B. Jemere, *Microchim. Acta*, 2019, **186**, 1–9.

65 X. Xu, S. Yang, Y. Wang and K. Qian, *Green Anal. Chem.*, 2022, **2**, 100020.
66 H. Park, M. K. Masud, J. Na, H. Lim, H.-P. Phan, Y. V. Kaneti, A. A. Alothman, C. Salomon, N.-T. Nguyen, M. S. A. Hossain and Y. Yamauchi, *J. Mater. Chem. B*, 2020, **8**, 9512–9523.
67 H. Malekzad, P. S. Zangabad, H. Mirshekari, M. Karimi and M. R. Hamblin, *Nanotechnol. Rev.*, 2017, **6**, 301–329.
68 A. Kumar, B. Purohit, P. K. Maurya, L. M. Pandey and P. Chandra, *Electroanalysis*, 2019, **31**, 1615–1629.
69 Y. Huang, P. Kannan, L. Zhang, T. Chen and D.-H. Kim, *RSC Adv.*, 2015, **5**, 58478–58484.
70 J. Sabaté del Río, O. Y. Henry, P. Jolly and D. E. Ingber, *Nat. Nanotechnol.*, 2019, **14**, 1143–1149.
71 H. Ishikura, Y. Fukasawa, K. Ogasawara, T. Natori, Y. Tsukada and M. J. C. Aizawa, *Cancer*, 1985, **56**, 840–848.
72 H. Ishikura, Y. Fukasawa, K. Ogasawara, T. Natori, Y. Tsukada and M. Aizawa, *Cancer*, 1985, **56**, 840–848.
73 G. Li, *Nano-inspired biosensors for protein assay with clinical applications*, Elsevier, 2018.
74 J. Upan, N. Youngvises, A. Tuantranont, C. Karuwan, P. Banet, P.-H. Aubert and J. Jakmunee, *Sci. Rep.*, 2021, **11**, 1–9.
75 S.-S. Li, Y.-Y. Tan, Y. Zhang, M. Liu and A. Liu, *Bioelectrochemistry*, 2021, **140**, 107804.
76 J. Mu, Y. Wang, M. Zhao and L. Zhang, *Chem. Commun.*, 2012, **48**, 2540–2542.
77 L. Liu, L. Tian, G. Zhao, Y. Huang, Q. Wei and W. Cao, *Anal. Chim. Acta*, 2017, **986**, 138–144.
78 A. Roberts, S. Mahari, D. Shahdeo and S. Gandhi, *Anal. Chim. Acta*, 2021, **1188**, 339207.
79 M. Hu, L. Zhu, Z. Li, C. Guo, M. Wang, C. Wang and M. Du, *Appl. Surf. Sci.*, 2021, **542**, 148586.
80 K. Mallikarjuna, Y. V. M. Reddy, B. Sravani, G. Madhavi, H. Kim, S. Agarwal and V. K. Gupta, *J. Electroanal. Chem.*, 2018, **822**, 163–170.
81 J. Zheng, H. Zhao, G. Ning, W. Sun, L. Wang, H. Liang, H. Xu, C. He and C.-P. Li, *Talanta*, 2021, **233**, 122520.
82 W. F. de Oliveira, P. M. dos Santos Silva, L. C. B. B. Coelho and M. T. dos Santos Correia, *Curr. Med. Chem.*, 2020, **27**, 3519–3533.
83 J. Feng, Y. Li, M. Li, F. Li, J. Han, Y. Dong, Z. Chen, P. Wang, H. Liu and Q. Wei, *Biosens. Bioelectron.*, 2017, **91**, 441–448.
84 Z. Huang, Z. Jiang, C. Zhao, W. Han, L. Lin, A. Liu, S. Weng and X. Lin, *Int. J. Nanomed.*, 2017, **12**, 3049.
85 F. Amiripour, S. N. Azizi and S. Ghasemi, *Biosens. Bioelectron.*, 2018, **107**, 111–117.
86 W. Liu, K. Hiekel, R. Hübner, H. Sun, A. Ferancova and M. Sillanpää, *Sens. Actuators, B*, 2018, **255**, 1325–1334.
87 N. Li, Y. Wang, Y. Li, W. Cao, H. Ma, D. Wu, B. Du and Q. Wei, *Sens. Actuators, B*, 2014, **202**, 67–73.
88 H. Lv, Y. Li, X. Zhang, Z. Gao, C. Zhang, S. Zhang and Y. Dong, *Biosens. Bioelectron.*, 2018, **112**, 1–7.
89 Q. Xu, H. Yuan, X. Dong, Y. Zhang, M. Asif, Z. Dong, W. He, J. Ren, Y. Sun and F. Xiao, *Biosens. Bioelectron.*, 2018, **107**, 153–162.
90 F. Liu, W. Deng, Y. Zhang, S. Ge, J. Yu and X. Song, *Anal. Chim. Acta*, 2014, **818**, 46–53.
91 A. Safavi and F. Farjami, *Biosens. Bioelectron.*, 2011, **26**, 2547–2552.
92 M. Wang, L. Yang, B. Hu, J. Liu, L. He, Q. Jia, Y. Song and Z. Zhang, *Biosens. Bioelectron.*, 2018, **113**, 16–24.
93 W. Mao, J. He, Z. Tang, C. Zhang, J. Chen, J. Li and C. Yu, *Biosens. Bioelectron.*, 2019, **131**, 67–73.
94 S. Ge, Y. Zhang, L. Zhang, L. Liang, H. Liu, M. Yan, J. Huang and J. Yu, *Sens. Actuators, B*, 2015, **220**, 665–672.
95 S. Barman, M. Hossain, H. Yoon and J. Y. Park, *Biosens. Bioelectron.*, 2018, **100**, 16–22.
96 M. Li, P. Wang, F. Pei, H. Yu, Y. Dong, Y. Li, Q. Liu and P. Chen, *Sens. Actuators, B*, 2018, **261**, 22–30.
97 Y.-C. Shi, A.-J. Wang, P.-X. Yuan, L. Zhang, X. Luo and J.-J. Feng, *Biosens. Bioelectron.*, 2018, **111**, 47–51.
98 J. Ribeiro, C. Pereira, A. Silva and M. G. F. Sales, *Biosens. Bioelectron.*, 2018, **109**, 246–254.
99 M. Sharifuzzaman, S. C. Barman, M. T. Rahman, M. A. Zahed, X. Xuan and J. Y. Park, *J. Electrochem. Soc.*, 2019, **166**, B983.
100 Z. Yuan, J. Chen, Y. Wen, C. Zhang, Y. Zhou, Z. Yang and C. Yu, *Biosens. Bioelectron.*, 2019, **145**, 111677.
101 B. Han, M. Pan, J. Zhou, Y. Wang, Z. Wang, J. Jiao, C. Zhang and Q. Chen, *Nanomaterials*, 2018, **8**, 724.
102 A. A. Abdelwahab, A. Elseman, N. Alotaibi and A. Nassar, *Microchem. J.*, 2020, **156**, 104927.
103 L. Fan, Y. Yan, B. Guo, M. Zhao, J. Li, X. Bian, H. Wu, W. Cheng and S. Ding, *Sens. Actuators, B*, 2019, **296**, 126697.
104 J. Jiao, M. Pan, X. Liu, B. Li, J. Liu and Q. Chen, *Sensors*, 2019, **20**, 71.
105 S.-Y. Cen, X.-Y. Ge, Y. Chen, A.-J. Wang and J.-J. Feng, *Microchem. J.*, 2021, **169**, 106568.
106 W. Dong, Y. Ren, Z. Bai, Y. Yang, Z. Wang, C. Zhang and Q. Chen, *Talanta*, 2018, **189**, 79–85.
107 X. Zhang, Y. Shen, Y. Zhang, G. Shen, H. Xiang and X. Long, *Talanta*, 2017, **164**, 483–489.
108 S. V. Piguillem, F. G. Ortega, J. Raba, G. A. Messina and M. A. Fernández Baldo, *Microchem. J.*, 2018, **139**, 394–400.
109 M. Aydın, E. B. Aydın and M. K. Sezgintürk, *Biosens. Bioelectron.*, 2018, **117**, 720–728.
110 H. Karimi-Maleh, A. Bananezhad, M. R. Ganjali, P. Norouzi and A. Sadrnia, *Appl. Surf. Sci.*, 2018, **441**, 55–60.
111 V. Arabali, S. Malekmohammadi and F. Karimi, *Microchem. J.*, 2020, **158**, 105179.
112 Z. Wang, S. Liu, P. Wu and C. Cai, *Anal. Chem.*, 2009, **81**, 1638–1645.
113 D. Du, X. Ye, J. Cai, J. Liu and A. Zhang, *Biosens. Bioelectron.*, 2010, **25**, 2503–2508.
114 Z. Lu, W. Dai, B. Liu, G. Mo, J. Zhang, J. Ye and J. Ye, *J. Colloid Interface Sci.*, 2018, **525**, 86–96.
115 H. Jia, J. Xu, L. Lu, Y. Yu, Y. Zuo, Q. Tian and P. Li, *Sens. Actuators, B*, 2018, **260**, 990–997.
116 J. Narang, N. Malhotra, C. Singhal, R. Bhatia, V. Kathuria and M. Jain, *Bioprocess Biosyst. Eng.*, 2017, **40**, 537–548.

117 Y. Liu and J. Yu, *Microchim. Acta*, 2016, **183**, 1–19.
118 M. Johari-Ahar, P. Karami, M. Ghanei, A. Afkhami and H. Bagheri, *Biosens. Bioelectron.*, 2018, **107**, 26–33.
119 Y. Zhao, Y. Tao, Q. Huang, J. Huang, J. Kuang, R. Gu, P. Zeng, H.-Y. Li, H. Liang and H. Liu, *Chemosensors*, 2022, **10**, 48.
120 S. Tang, W. Wu, X. Xie, X. Li and J. Gu, *RSC Adv.*, 2017, **7**, 9862–9871.
121 Y. Zhou, S. Yang, X. Yin, J. Han, M. Tai, X. Zhao, H. Chen, Y. Gu, N. Wang and H. Lin, *J. Mater. Chem. A*, 2019, **7**, 1878–1888.
122 L. T. Tufa, S. Oh, J. Kim, K.-J. Jeong, T. J. Park, H.-J. Kim and J. Lee, *Electrochim. Acta*, 2018, **290**, 369–377.
123 K. Navakul, C. Warakulwit, P.-T. Yenchitsomanus, A. Panya, P. A. Lieberzeit and C. Sangma, *Nanomedicine*, 2017, **13**, 549–557.
124 T. Yan-Bing, J. Huang, Z. Yu-Nong, C. Yan, Q. Huang, S. Bo-Xiang, C. Jian-Jun and L. Huan, *Chin. J. Anal. Chem.*, 2022, **50**, 53–59.
125 S. Huang, W. Wang, J. Li, T. Zhang, Y. Liang, Q. Wang and Z. Jiang, *Chem. Eng. J.*, 2021, **419**, 129613.
126 L. Wu, E. Xiong, X. Zhang, X. Zhang and J. Chen, *Nano Today*, 2014, **9**, 197–211.
127 S. Biswas, Q. Lan, Y. Xie, X. Sun and Y. J. A. A. M. Wang, *ACS Appl. Mater. Interfaces*, 2021, **13**, 3295–3302.
128 M. Coculova, D. Imrichova, M. Seres, L. Messingerova, V. Bohacova, Z. Sulova and A. Breier, *Leuk. Res.*, 2016, **48**, 32–39.
129 P. Gulati, P. Kaur, M. Rajam, T. Srivastava, P. Mishra and S. Islam, *Anal. Biochem.*, 2018, **557**, 111–119.
130 M. H. Jazayeri, H. Amani, A. A. Pourfatollah, H. Pazoki-Toroudi and B. Sedighimoghaddam, *Sens. bio-sens. Res.*, 2016, **9**, 17–22.
131 Y. Wang, J. Luo, J. Liu, X. Li, Z. Kong, H. Jin and X. Cai, *Biosens. Bioelectron.*, 2018, **107**, 47–53.
132 P. Bollella, G. Fusco, C. Tortolini, G. Sanzò, G. Favero, L. Gorton and R. Antiochia, *Biosens. Bioelectron.*, 2017, **89**, 152–166.
133 M. Wang, L. Yang, B. Hu, J. Liu, L. He, Q. Jia, Y. Song and Z. J. B. Zhang, *Biosens. Bioelectron.*, 2018, **113**, 16–24.
134 S. Su, X. Han, Z. Lu, W. Liu, D. Zhu, J. Chao, C. Fan, L. Wang, S. Song and L. Weng, *ACS Appl. Mater. Interfaces*, 2017, **9**, 12773–12781.